Molecular Crystals and Liquid Crystals
Publication details, including instructions for authors and subscription information:
http://www.tandfonline.com/loi/gmcl20

Liquid Crystals Under Two Extremes: (1) High-Power Laser Irradiation, and (2) Single-Photon Level

Svetlana G. Lukishova [a]
[a] The Institute of Optics, University of Rochester, Rochester, NY, 14627-0186, USA

Version of record first published: 11 May 2012.

To cite this article: Svetlana G. Lukishova (2012): Liquid Crystals Under Two Extremes: (1) High-Power Laser Irradiation, and (2) Single-Photon Level, Molecular Crystals and Liquid Crystals, 559:1, 127-157

To link to this article: http://dx.doi.org/10.1080/15421406.2012.658703

Mol. Cryst. Liq. Cryst., Vol. 559: pp. 127–157, 2012

ISSN: 1542-1406 print/1563-5287 online
DOI: 10.1080/15421406.2012.658703

Taylor & Francis
Taylor & Francis Group

Liquid Crystals Under Two Extremes: (1) High-Power Laser Irradiation, and (2) Single-Photon Level

SVETLANA G. LUKISHOVA*

The Institute of Optics, University of Rochester, Rochester, NY 14627-0186, USA

This paper describes some of my results on liquid crystal investigations under unconventional, incident light powers: (1) under high-power laser irradiation both in free space and inside laser resonators, and (2) in single-photon source applications for quantum information technology. Several effects under high-power, nanosecond laser irradiation are outlined: athermal helical pitch dilation and unwinding of cholesteric mirrors, showing the limits for using them in laser physics; some pitfalls in measurements of thermal-density refractive nonlinearity and the first observation of thermal lens effects in liquid crystals under several nanosecond, low-pulse-repetition rate (2–10 Hz) laser irradiation in the presence of two-photon absorption; feedback-free kaleidoscope of patterns (hexagons, stripes, etc.) in dye-doped liquid crystals. At the single-photon level, definite linear and circular polarizations of single (antibunched) photons for quantum communications were obtained using single-emitter fluorescence in planar-aligned nematic and cholesteric hosts. Circular polarized cholesteric microcavity resonances were also observed under cw-excitation. In addition, using near-field optical microscopy and AFM, 2D-hexagonal arrays made of cholesteric oligomers were investigated. With progress of this technology, similar arrays can be used for fluorescence control of single emitters.

Keywords Helix unwinding; liquid crystals; nonlinear refraction; single-photon source

Introduction

The development of liquid-crystal optics for high-power lasers began in 1979 at the Laboratory for Laser Energetics (LLE), University of Rochester, when it became apparent that some optical-component requirements of large-aperture solid-state lasers for thermonuclear fusion could not easily be met by solid-crystalline materials [1–3]. One such component, a high-quality, laser-beam apodized aperture has been the goal of solid-state laser fusion research programs both in the US and USSR since the early 1970's [1,4]. I worked at the Soviet/Russian Academy of Sciences (Moscow) on high-damage threshold apodized apertures and graded reflectivity mirrors [4–8] for reducing small-scale self-focusing effects [4,9] in high-power laser fusion systems and for improving the beam quality of industrial lasers [8]. To learn from the experience in *high-damage threshold* liquid crystal (LC)

*Address correspondence to Svetlana G. Lukishova, The Institute of Optics, University of Rochester, Rochester, NY 14627-0186, USA. Phone: 585/276-5283; Fax: 585/244-4936. E-mail: sluk@lle.rochester.edu

apodizing devices [1] and cholesteric mirrors [10–15], I visited LLE in 1993. Crucial in the preparation of LC materials with *high-damage threshold* under high-power laser irradiation is the purification of "as received" liquid crystals (LCs) through filtration to remove condensation centers for laser-induced bubble formation on the surface of the LC cell. It should be pointed out that high-power laser applications of LCs are not the principal sector among all LC applications. Commercial vendors of LCs are therefore unlikely to provide materials optimized for high-power-laser use. That is why two types of possible contributors to laser damage of LC materials must be avoided. They are undissolved extrinsic impurities that can be removed using particle filters and intrinsic impurities (dissolved gaseous components that can be removed by degassing as well as synthesis byproducts or catalyst traces that can be removed by chromatography). In Refs. 1–3 it was shown that after purification of the "as received" LC samples the laser-damage threshold for massive material modification (visible burst of stable bubbles and glass chips in the cell surface and/or a web of scatter lines) improved sharply. For purified (using 0.2-μm particle filter) and degassed, isotropic 5CB, thresholds for permanent photolysis at $\sim$9.6 J/cm^2 and $\sim$4.4 J/cm^2 were observed under single and multiple shots respectively (1 ns pulse duration, 1-mm beam diameter, wavelength $\lambda = 1.053$ μm). Under similar conditions, transient-bubble "damage" observable under 110 x dark-field magnification in "as received" LCs occurred at $\sim$0.76 J/cm^2 for isotropic 5CB and $\sim$ 0.89 J/cm^2 for isotropic E7 (single-shot threshold) [1,3,16].

A similar problem in purification of "as received" LC materials arises when the LC is used as the host for single-emitters. In this case, single-photon counting detectors can detect fluorescence from impurities in the LC material itself [17] instead of fluorescence from a particular single emitter. In addition, for some types of single emitters it is desirable to avoid oxygen, the singlet-state of which can contribute to single-emitter bleaching. Removing the oxygen from a monomeric LC by saturation with helium or argon gas permitted us to record cw-excitation fluorescence from single dye molecules without bleaching for more than 1 hour [18,19].

The structure of this paper is as follows. It consists of two parts. Part 1 is an overview of my research on LCs under high-power laser irradiation. Chapter 1.1 of this part is devoted to my Moscow research at the Institute of Radio Engineering and Electronics of the Russian Academy of Sciences on athermal cholesteric pitch dilation and unwinding of cholesteric liquid crystal (CLC) mirrors by the field of a light wave. These experiments were carried out both in free space and with the CLC mirror as the output coupler of a laser resonator. Special conditions of experiments permitted to prove that this effect is not connected with heating. I used purified CLC material provided by A.W. Schmid (LLE, University of Rochester). CLC mirrors were prepared by S.V. Belyaev's group of the Moscow Organic Intermediates and Dyes Institute NIOPIK. Two of my students of the Moscow Institute of Physics and Technology (FizTech), K. Lebedev and E. Magularia participated in this project. The research was supported by Grants of the International Science (Soros) Foundation, the Russian Government, and the Russian Foundation for Basic Research.

Chapter 1.2 is devoted to some of my results obtained at the Liquid Crystal Institute, Kent State University, on nonlinear absorption and refraction of cyanobiphenyl liquid crystals to high-power, several-nanosecond laser irradiation, using z-scan measurements. Two effects were observed under conditions of two-photon absorption: dependence of nonlinear refraction on laser-beam diameter (thermal-density nonlinearity) and the first-time observation of a thermal-lens in LCs under several nanosecond irradiation and low-pulse-repetition rate. This work was made possible by the hospitality of P. Palffy-Muhoray and with the help of T. Kosa and B. Taheri.

Chapter 1.3 is devoted to feedback-free pattern formation using highly absorbing dye-doped nematic liquid crystals. This work was carried out at the Institute of Optics, University of Rochester, owing to the hospitality of R.W. Boyd and with the help of K. Marshall and N. Lepeshkin.

Part 2 of this paper describes my investigation, at the single-photon level, of LCs doped with single emitters (dye molecules, nanocrystal quantum dots, and color centers in nanodiamonds). To my knowledge, this is the first research on LCs at the single-photon level. Chapter 2.1 describes a single-photon source for quantum communication with definite circular polarization of single photons using a CLC. The results on circularly polarized microcavity resonances are also presented here. Chapter 2.2 is devoted to a single-photon source with definite linear polarization using nematic LC. Chapter 2.3 discusses near-field optical microscopy of defects in oligomeric CLCs. Defects were prepared as 2D-hexagonal arrays with periodicities of the order of visible-light wavelengths. With some improvement of the described technology, similar arrays can be used for fluorescence control of single emitters. These projects supported by ARO and three NSF grants as well as Air Force and NASA graduate student fellowships, were carried out at the Institute of Optics, University of Rochester. My Ph.D. students L.J. Bissell [20] and J.M. Winkler as well as undergraduates C. Supranovich, R. Knox and summer research associate P. Freivald contributed to this project. I also used help and advice of K. Marshall, A.W. Schmid, L. Novotny, and A. Lieb. Some oligomeric CLC material was synthesized by S.-H. Chen's group, some nanocrystal quantum dots were synthesized by T. Krauss' group. C.R. Stroud and R.W. Boyd contributed in discussions of the results.

1. Liquid Crystals Under High-Power Laser Irradiation

1.1. Athermal Cholesteric Pitch Dilation and Unwinding by the Field of a Light Wave

In 1982, Winful determined that athermal, light-induced changes in the pitch of the cholesteric helix lead to a reflectivity drop of a CLC mirror in the region of selective reflection [21]. However, later attempts [22,23] at detecting this effect in laser fields remained unsuccessful, in spite of the fact that chiral unwinding under the influence of both static and time-varying *electric* and *magnetic* fields had been observed. The challenge in observing *athermal* helix pitch dilation and its unwinding by *optical* fields arises from the larger than $E \sim 10^4$ V/cm electric-field strength requirement on the optical wave that needs to act on the CLC for time periods commensurate with the characteristic unwinding time of the helix $t_h \sim$ several milliseconds. Therefore, neither short-pulse intensities [22,23] exceeding by an order of magnitude Winful's estimation nor rather low intensities applied cw [10–13], succeeded in triggering nonlinear changes in the reflectivity of nonabsorbing CLC mirrors. In a series of reports [10–13], only changes in curvature and improvement of the transverse beam profile of CLC mirrors were demonstrated in a cw-laser beam.

The first athermal drop in CLC mirror reflectivity in response to strong, circular polarized laser radiation was observed by my group in 1995 [24–28]. A special laser operating mode was selected using a pulsed, 4.5 kHz pulse-repetition-rate laser with an accumulation effect from many pulses. The effect was observed both in free space [24,25,27,28] and inside a laser resonator [24,26,27,28] with a CLC mirror as the output coupler. To distinguish a field-induced orientational effect from thermal changes of the cholesteric pitch, the laser was switched to cw-operation with the same average intensity as in the pulsed regime. The effect was only observed at pulsed irradiation and depended only on peak intensity, but

not on average intensity. The effect was demonstrated in four CLC mirrors with different substrate-surface-treatment methods for planar alignment. Sections of this Chapter 1.1 are devoted to the details of the experiments and their discussions.

It should be noted, that the authors of Ref. 29 also observed nonlinear selective reflection effects using the property of CLCs to achieve faster orientational response time to high-intensity beams. At incident, single-pulse peak intensities of $\sim$GW/cm^2, the CLC mirror reflectivity dropped from 90 to 25% even for single, nanosecond pulses. In paper [29], a CLC mirror was used in a resonator of an electrooptically Q-switched laser. It was shown that the light-induced reflectivity drop leads to passive cavity-dumping and an improved transverse beam profile.

1.1.1. Cholesteric Mirror Fabrication and Characterization. The CLC mirrors were prepared from a photochemically stable mixture of nematic E7 and the chiral twisting agent CB15 (both from Merck) with mix ratio adjusted for maximum reflectivity around the wavelength $\lambda = 1.064$ μm (21.4 wt% CB15 + 78.6% wt% E7). The mixture was prepared and filtered in a clean room at the LLE, University of Rochester. The average refractive index of the mixture was $n_{av} = 1.557$. The results of the spectrophotometric measurements of the transmission coefficients of three, sealed mirrors as a function of wavelength for nearly completely circular-polarized radiation using a quarter waveplate for 1.064 μm wavelength are presented in Fig. 1.

Planar alignment of the cells was achieved at the Moscow Organic Intermediates and Dyes Institute NIOPIK by the following methods. It is very important that at one inner side the CLC-cell LC molecules had strong anchoring. On the opposite inner side of the CLC cell, LC molecules had weak anchoring. For all mirrors, the side of the glass cell with strong-anchored director was polyimide coated and then rubbed. The weak-anchoring side was left unbuffed but covered with (1) polyimide only – mirror 1; (2) polyvinylcinnnamate and subsequent photoorientation – mirror 2; (3) polyvinylcinnnamate and subsequent photoorientation with additional shearing of the substrates – mirror 3; (4) polyimide only – mirror 4. The LC layer thickness in the hermetically sealed cells (1–3) were 12.8, 13.8, and 6.5 μm, respectively, and in the unsealed (open contact with air) cell (4) – 20 μm.

1.1.2. Cholesteric Mirrors in Free Space. Experimental set up for irradiation of a CLC mirror by a freely propagating laser beam is shown in Fig. 2. We used a Nd:YAG laser with 1.064 μm wavelength. In this spectral region, no two-photon absorption effects in the

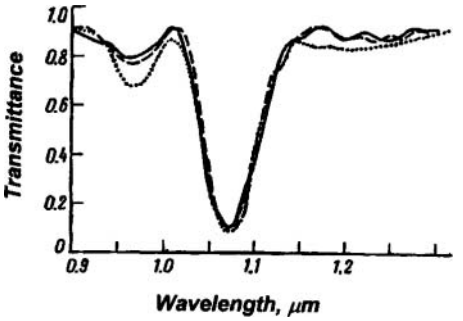

Figure 1. Spectral transmittance of three CLC mirrors using a quarter waveplate for $\lambda = 1.064$ μm.

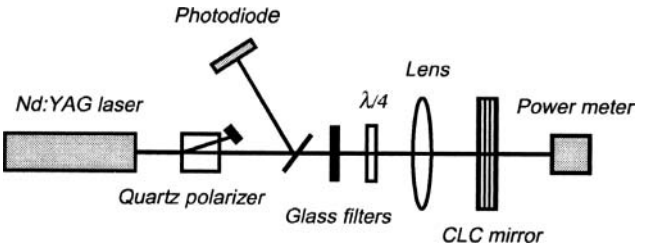

Figure 2. Experimental setup for free-space experiments with CLC mirrors.

CLC material should be observed. The laser operated in two regimes: (1) in cw mode and (2) in an acousto-optically Q-switched mode, emitting high-repetition-rate (4.5 kHz) pulse trains, each pulse being 500 ns long. In either mode, the average power reaching the CLC samples was between 0.3 and 1 W. Beam cross-sections before focus were monitored by a CID camera and video processing setup. From the recorded beam profiles, $1/e^2$ intensity beam diameters of between 50 and 200 μm were derived, corresponding to sample-plane peak-intensities (for 500-ns pulses) of 10^6–10^7 W/cm^2.

Upon focusing of free-space-propagating, 500-ns, 4.5-kHz-repetition-rate pulses into the CLC layer, we observed an increase in CLC-mirror transmittance of between 5% and 30-80%. This reflectivity drop appeared within 1 to 10 min from the onset of irradiation (Fig. 3), depending on the specific mirror. Interestingly, this effect did not depend on the magnitude of the average-intensity. Under cw irradiation conditions, we did not observe any effect even at average intensities twice as large as the average intensities in the pulsed, high-repetition rate mode. Furthermore, the effect appeared only, even in the case of high-repetition-rate pulse irradiation, under reflection of the incident light from the *strong-anchoring* side of the CLC mirror. Under 180° reversal, i.e., with the weak-anchoring side facing the incident beam, we did not observe any effect. The temperature drift in selective reflection for our given CLC mixture is estimated at $+1$ nm/C°, requiring a temperature excursion of more than 50 C° to account for the $\sim$70% change in CLC-mirror transmittance at 1.064 μm. We did not observe such heating in the present CLC cells.

A recovery of the mirror reflectivity to its prior condition appeared after either terminating irradiation or switching it to cw-mode.

1.1.3. Cholesteric Mirrors in Laser Resonators. For the laser-resonator studies, a plane-parallel cavity of the same laser used in section 1.1.2 was formed by a dielectric hard mirror and a CLC output coupler (Fig. 4). An active Nd:YAG element was pumped by a continuously operating arc flashlamp filled with krypton (the voltage across this lamp was

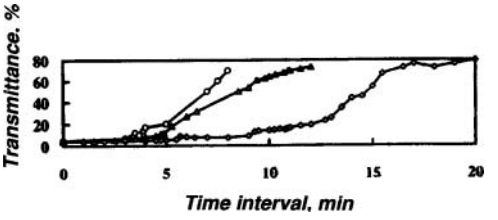

Figure 3. Dependence of CLC mirror transmittance on irradiation time under high- repetition-rate, pulsed irradiation at different incident intensities.

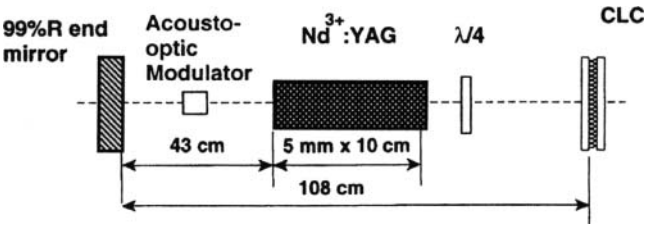

Figure 4. Schematic of the CLC-mirror-equipped laser oscillator.

100 V). Pumping of the active element generated a thermal lens whose optical power was +1 dioptre/kW. Switching to high pulse-repetition rate operation (500 ns pulse duration, 4.5 kHz pulse repetition rate) was performed by an acousto-optical switch. A quartz quarter waveplate was placed inside the resonator between the active element and the CLC output coupler. The diameter of the optical beam at the laser output was ∼0.8 mm at an average output power of 1 W. No significant difference was observed between the slope efficiency of the laser with conventional dielectric or CLC output mirrors when the reflection coefficients were the same. The advantage of the CLC mirror was a lower sensitivity of the laser operation to cavity misalignment. At cw-operation and at low pumping rate in the pulsed high-repetition-rate regime, the slope efficiency and the lasing stability were the same for laser with CLC and dielectric mirrors. At high flashlamp currents, the average output power obtained in the high-repetition-rate mode decayed rapidly and disappeared after 0.5–5 min from switching, but only when the side of the CLC mirror with strong surface anchoring was facing the gain medium. The pump threshold (i.e., the current to the flashlamp) at which lasing was suppressed was different for each CLC mirror. It was 28.5–29.5 A for the output mirrors 1–3 with reflection coefficient $R = 95\%$, and ∼24.5 A for the CLC mirror 4 with $R = 85\%$.

Figure 5 depicts the time dependence of the laser output power obtained for two CLC mirrors when a change from the cw to the pulsed regime occurred at high flashlamp currents. Turning on the acousto-optical switch (at t_1) quenched the lasing action because of a drop in the reflection coefficient of the CLC mirror. Turning off the switch (at t_2) gradually restored

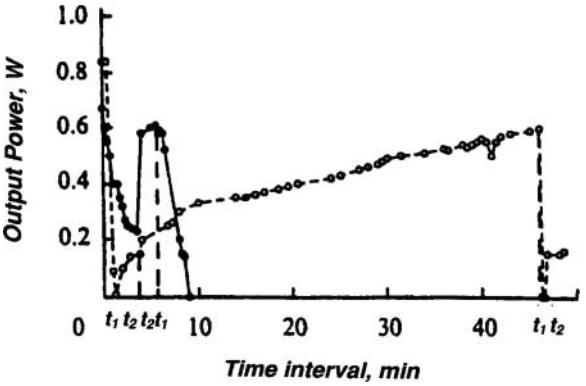

Figure 5. Time dependence of the average output power of a CLC-mirror laser with changing the operating regime from cw to high-repetition rate (t_1) and back (t_2). Solid and dashed curves present results for different mirrors.

the lasing action. A second change to the pulsed regime suppressed lasing again and it was restored when the laser was made to operate in the cw-mode again.

1.1.4. Discussion of the Results on Nonlinear Selective Reflection of CLC Mirrors. The observed reflectivity drop of CLC mirrors may be interpreted within the frame of the chiral pitch-dilation model, in which helix deformation [30] takes place under the influence of a high-intensity (1 to 10 MW/cm^2) light field. In accordance with the derivations in Ref. 21, the critical field strength for helix unwinding to "thick" CLC layers of thickness $L > 2\lambda/(\pi\,\Delta n)$ takes on the form

$$|E|_{cr}^2 = 4\pi(\omega/c)^2(\varepsilon_a/\varepsilon)K_{22}, \tag{1}$$

where $\varepsilon \sim n_{av}^2$, and the optical-regime dielectric anisotropy ε_a is

$$\varepsilon_a = \varepsilon_e - \varepsilon_o = n_e^2 - n_o^2 \sim 2\Delta n n_{av}. \tag{2}$$

Substituting the approximation (2) into (1), yields

$$|E|_{cr}^2 = (32\pi^3 K_{22}/\lambda^2)(\Delta n/n_{av}). \tag{3}$$

For $\lambda = 1.064$ μm, $\Delta n = 0.174$, $n_{\mathrm{av}} = 1.6$, and $K_{22} = 5 \times 10^{-7}$ dyne, the critical-field value becomes $E_{cr} = 2.1 \times 10^4$ V/cm, but $2\lambda/(\pi\,\Delta n) = 3.9$ μm, i.e., considerably smaller than L for any of our CLC mirrors. Under our experimental conditions the field strength E at the beam center is 2.2 to 7×10^4 V/cm, i.e., larger than E_{cr}.

Note that helix unwinding by a light field under selective reflection conditions *differs from unwinding in a low-frequency field* for which $E_{cr} \sim \varepsilon_{\mathrm{a}}{}^{-1}$ [31–33]. In the circularly polarized light field the electric-field vector changes direction throughout the CLC-layer thickness (while the low-frequency-field vector orientation remains fixed), suffering an exponential drop in magnitude over the critical length $L_{cr} \sim \varepsilon_{\mathrm{a}}{}^{-1}$ and, thus, remaining unable to "see" further into the CLC layer [21]. A comparison of our results with those on helix pitch dilation in a low-frequency field directed along the plane of a planar-alignment of a CLC layer [31–34] shows our optical field strength to considerably exceed the value of $\sim 10^4$ V/cm proven adequate [31–34] for helix untwisting at low frequencies.

In Ref. 35 for a low-frequency field, the field-induced pitch changes relaxed in a spatially non-monotonous, step-wise fashion, owing to the particular field gradient chosen and double-sided strong anchoring of the cell. As shown in Fig. 3 (see also Ref. 28), our CLC mirrors' optical transmission-coefficient dependence on irradiation time is non-monotonous as well, although individual unwinding steps are in these graphs "blurred" by the experimentally necessitated spatial integration of the effect over the excitation beam's radial intensity distribution. Deformation energy is accumulated in the CLC layer over the interaction time of a single laser pulse (500 ns), and this energy is partially dissipated during the "quiet" period between the pulses (200 μs), since the relaxation time of the deformed helix is of the order of 1000 μs. Therefore, the unwinding of the cholesteric helix in an optical field occurs only over quite a long time (accumulation of nonlinear changes) during pulsed high-repetition rate laser irradiation.

1.2. Thermal-Density Nonlinearity and Thermooptical Effects in Liquid Crystals Under High-Power, Several Nanosecond Laser Irradiation

In this Chapter, I will briefly overview some of my results on nonlinear optical response of cyanobiphenyl LCs to high-power, nanosecond laser irradiation which I obtained at the

Liquid Crystal Institute, Kent State University in 1997–1998. My full review on this subject including other group results is published in [28]. I would like to emphasize two important results which were overlooked in the past in z-scan measurements of LCs in the presence of nonlinear absorption: (1) for isotropic LCs at several-nanosecond time scale and several tens-micrometers beam-waist-diameter the influence of coupled thermal and density effects on nonlinear refraction depends, through buildup time, on *the beam-waist diameter*; (2) for planar nematic layers, *cumulative effects* in heating (and in refractive nonlinearity) were observed even at low, 2–10 Hz pulse repetition rate. These results are important for optical power limiting and switching applications, and for intensity and beam-quality sensors of pulsed, high-power lasers.

Heating of cyanobiphenyl LCs by short-pulse laser radiation in the visible range that drives photoacoustical (thermal-density) and thermooptical effects, is caused by two-photon absorption [36,37], concurrent or subsequent excited state absorption [36,38–40], and the efficient decay of the excited states through radiationless-recombination channels [36,38–40]. Strong nonlinear absorption in the visible was observed in optical power limiting studies of LCs [41–49] and in z-scan measurements [50–55]. For the nematic phase, the two-photon absorption coefficient has a several-times-higher value for incident polarization parallel to the molecular dipole direction than for perpendicular polarization [37].

As in any absorbing medium, in the presence of nonlinear absorption, the thermal mechanism causes refractive nonlinearity in nematic and isotropic LCs. The thermal nonlinearity coupled to density changes [41,42] (which is negative) competes with the orientational (positive) nonlinearity in changing the sign of the total refractive nonlinearity [28]. Another mechanism of density changes, electrostriction, with buildup time in the nanosecond range, is comparable to thermal/density contributions if medium absorption coefficients are low. At 0.532 μm a strong heating mechanism exists for the monomeric LCs as a result of two-photon and excited state absorption. That is why electrostriction is neglected in these experiments.

Refractive index changes by heating are the sum of two contributions:

$$\Delta n = (\partial n/\partial \rho)_T \Delta \rho + (\partial n/\partial T)_\rho \Delta T, \tag{4}$$

where ρ is the density, T is the temperature. It is very important in the current context that each term in (4) has its own turn-on time, and will contribute differently under transient and steady-state regimes [28,56–58].

1.2.1. Thermal-Density Nonlinearity $(\partial n/\partial \rho)_T \Delta \rho$*).* For several-nanosecond pulse duration and several tens of micrometers beam waist, the buildup time t_{ac} of the thermal-density nonlinearity ($\Delta n = (\partial n/\partial \rho)_T \Delta \rho$) can be close to the laser pulse duration t_o :

$$t_{ac} = r_o / V_s, \tag{5}$$

where r_o is the beam radius and V_S is the velocity of sound (V_S (LCs) ~1500 m/s). For $t_{ac} > t_o$ the thermal-density-nonlinearity will not develop during the pulse. Experimental values of nonlinear refractive index n_2 for this transient regime were reported in Ref. 56 for absorbing organic liquid. It was found experimentally, that the transient absolute value of n_2 for $t_o = 5$ ns diminishes with r_o increasing from 9 to 32 μm. (The value of n_2 is defined in our paper by $n = n_0 + 1/2\ n_2|E|^2$). In a series of papers [57,58] numerical modeling was carried out for this regime. Acoustic grating generation in LCs have been intensively studied both under subpico-, pico- and nanosecond excitation [36,38–42].

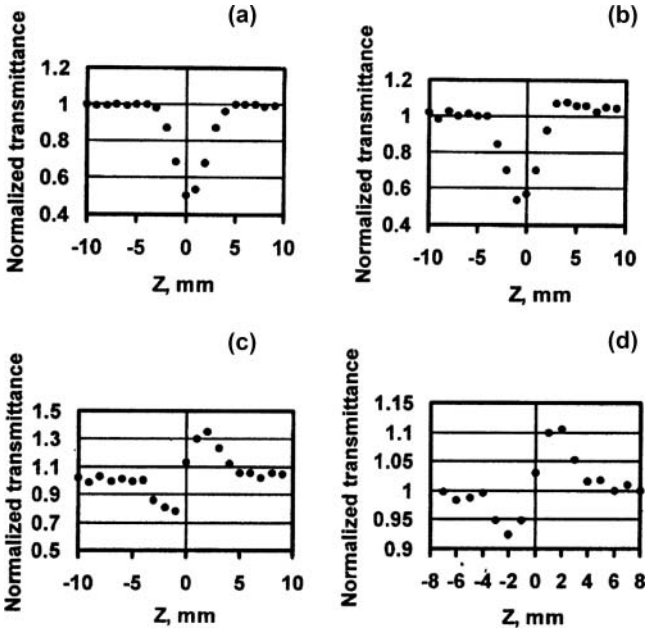

Figure 6. Z-scan curves for isotropic 5CB: (a) open aperture; (b) closed aperture; (c) closed/open aperture; and (d) closed aperture for CS_2.

The typical z-scan curves of *transient* nonlinear refraction of room-temperature CB15 samples with 2-mm thickness for 0.532 μm laser excitation [28,59] are presented in Fig. 6(a)–(c) for incident intensity $I = 0.74$ GW/cm^2. For comparison, a z-scan curve for CS_2 with 2-mm thickness is presented as well (Fig. 6(d)) for $I = 0.73$ GW/cm^2. The results from these curves yield the following values [28]: $n_2(\text{CB15}) = 2.5\, n_2\,(\text{CS}_2)$. Beam-waist diameter was $\sim$36 μm, and $t_o = 6.8$ ns, 10-Hz pulse repetition rate. The aperture factor for these z-scan measurements was S$\sim$0.1 [28]. For isotropic 5CB with 2-mm-cell thickness under similar conditions in the temperature interval 35.6–50°C, the *transient* value of n_2(5CB) varied from 2.5 to $3.7n_2(\text{CS}_2)$. In both cases, isotropic 5CB and CB15, self-focusing (converging lens) was observed. The absolute value of $n_2(\text{CS}_2)$ for these conditions is equal to 1.2×10^{-11} esu [60]. In papers [50,55] for 7-μm diameter measurements, negative values of n_2 (self-defocusing) were reported for isotropic 5CB using the same laser. This difference is explained by the dependence of the value of transient thermal-density nonlinearity with negative sign on the beam-waist diameter. For 7-μm diameter, t_{ac} is less than the pulse duration time and nonlinear refraction as a result of density changes prevails under the positive-sign, transient, orientational nonlinearity.

1.2.2. Thermooptical Effects $(\partial n/\partial T)_p \Delta T$) as the Result of Cumulative Effects in Heating of Planar-Aligned LC-Cells. The thermooptic coefficient *dn/dT* in nematic LCs is extraordinarily large, ranking among the largest of all known materials [61]. Not unexpected for these highly anisotropic molecules, it depends on the orientation of the molecules. E.g., dn_{par}/dT was reported [62] of $\sim 2.5 \times 10^{-3}$ grad^{-1} for 5CB in the temperature interval 26–31°C for incident linear polarization parallel to the molecular orientation direction. For "perpendicular" polarization, dn_{perp}/dT is of opposite sign and equals $\sim -1/2\, dn_{par}/dT$ [61].

In the proximity of the phase transition to the isotropic state, the slope of both dn_{par}/dT and dn_{perp}/dT steepens [62].

For nematic LCs, it is well-known that the thermooptical effect experiences a lengthening of its buildup time (tens-hundreds of nanoseconds), rendering it insignificant on a several-nanosecond time scale [41,42]. Similar buildup times are reported in Ref. 56 for an absorbing organic fluid. Thermooptical effects for $r_o = 32$ μm were found to be more significant for pulses longer than ~100 ns [56].

Because of the slow buildup time, thermooptical (thermal-lens) spatial self-phase-modulation rings in the beam cross-section were observed only for cw laser radiation [63–65]. LC heating was in this case due to absorbing coatings on cell glass-substrates, dissolving absorbing dyes in LCs, and/or irradiation of unpurified LCs by high-average power (~1W for 100-μm spot size [63]) beams.

For pulsed lasers the first report on thermal-lens spatial self-phase-modulation rings was published in my papers [28,66,67]. I irradiated a planar-aligned nematic cell with a 0.532-μm laser beam (7 ns pulse duration, 10 Hz pulse repetition rate), propagating perpendicular to the cell walls. Linear polarization of the beam was parallel to the alignment direction of the LC molecules. In this configuration, no orientational effects should be observed. Over time spans of ~0.5–ten seconds high-contrast, concentric, elliptical diffraction rings appeared in the far-field (Fig. 7) whose major axes orient themselves perpendicular to the incident polarization direction. Once formed, each set of rings may remain stable for up to several minutes. Upon continued pulsed irradiation over several minutes, the number of these rings varies systematically with laser intensity (sometimes between 1–2 and (up to) 20 rings). This ring pattern (see Fig. 8) differs from that typically obtained from orientational spatial self-phase modulation. In our case, the ring pattern evolves under polarization conditions for which, in principle, no orientational effects may occur (polarization of laser light is parallel to the director orientation). Under cw-irradiation at twice the average intensity than the average intensity under pulsed irradiation, the effect fails to exist. The key characteristics of the effect are as follows:

- This effect and its development exhibit threshold behavior depending on both the incident peak intensity and the geometry of irradiation, but not on the average intensity.
- The effect's evolution depends on the irradiation geometry (focal beam diameter) and, for a given geometry, on the cell thickness.
- The effect exists at both 2-Hz and 10-Hz pulse repetition rate, however, in the 2-Hz case the threshold increases (cumulative effect).
- Adding a two-photon absorbing chromophore does not change the character of the effect, but only lowers its threshold by ~2–2.5 times (for the tested chromophore type and concentration).

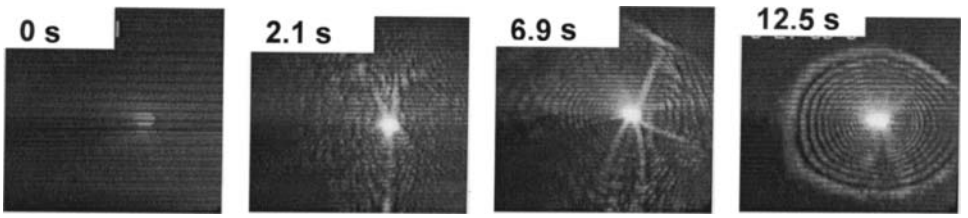

Figure 7. Time evolution of the elliptical ring pattern in the far-field (development of a thermal lens).

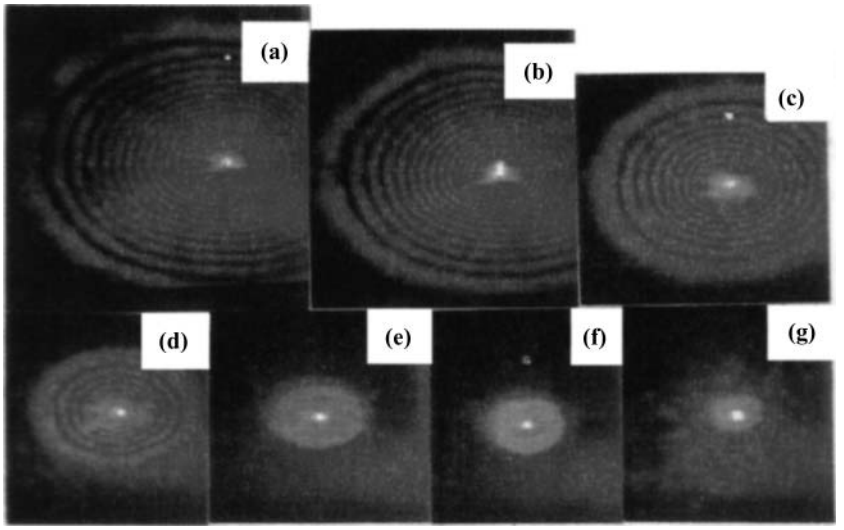

Figure 8. Set of elliptical ring patterns with diminishing incident intensities from (a) to (g).

- When the LC cell was rotated around the light-propagation direction, the elliptical rings' major and minor axis rotated in the same handedness, but the number of rings diminished as the angle between LC director and incident linear polarization increased. However, when the LC director was oriented perpendicular to the light polarization, the effect vanished entirely at incident intensities below $\sim$1 GW/cm^2.

Figures 7 and 8 show the effect development for a large-beam diameter (slow focus). At 160μm beam diameter, a cell thickness of 25–50 μm did not permit evolution of the effect (only chaotic break-up of the beam was observed), while larger-thickness (105–125 μm) cells did. The elliptical ring patterns developed from the original beam spot through several "rays" of scattered light (Fig. 7). Images in Fig. 7 (105-μm layer thickness of 5CB and 7CB mixture with two-photon absorbing chromophore, $I = 0.5$ GW/cm^2) were obtained by recording from the screen elliptical ring patterns onto magnetic tape at full repetition rate, and digitizing each frame afterwards.

Figure 8 shows the evolution of the ring-pattern with diminishing incident intensity for layer thickness 125 μm. As well as in Fig. 7, for lowering the effect threshold doping of the mixture of 5CB and 7CB LCs with the two-photon absorbing chromophore was used (it has no linear absorption at this wavelength). The same patterns were observed in pure 5CB (or mixture with 7CB), but at incident intensity levels twice larger than used here. In these experiments I used chromophore bis[di-n-butylamino]stilbene provided by J. Perry.

For tight focusing (35–50 μm beam-waist diameter), the effect of elliptical ring formation was observed for all used cell thicknesses (25–30, 50, 105, 125 μm). In my paper [28], tight-focusing experiments without using two-photon absorbing chromophores were described in details. Several new spatial patterns ("dark" spot formation, asymmetric scattering, "cross" formation) were observed in this case.

For explanation of the slow buildup time spatial self-phase modulation as well as its absence under cw irradiation of comparable average intensity, the heating of LC under *two-photon absorption* conditions was further scrutinized. Assuming that the glass substrates do not absorb at all, numerical solutions have been sought for the heat balance equation.

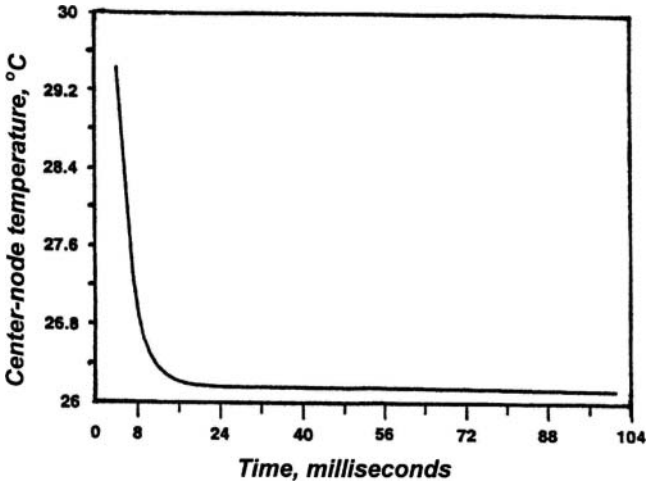

Figure 9. Numerical modeling of the heat diffusion: center-node temperature relaxation in time after the first pulse.

The finite-element solutions were obtained using the commercial ANSYS/Thermal code, including thermal conduction in the LC-material and the two glass-walls of the LC-cells, convection from the glass walls to air, and enthalpy effects at the phase-transition temperature. Two-dimensional transient thermal analysis was carried out for the initial condition of a Gaussian spatial temperature distribution written by the laser pulse with 10 Hz pulse repetition rate into the material. Temperature-dependent material parameters for 5CB (thermal conductivity, specific heat) were provided in file form by the authors of Ref. 68. The details of this modeling made by A. W. Schmid are presented in paper [28] for the in-focus $1/e^2$ laser-beam diameter of 160 μm, LC layer thickness of 125 μm, glass substrate thickness of 375 μm, room temperature $T_{\text{room}} = 26^\circ$C. Figure 9 shows temperature relaxation with time after the first pulse at the central node of the 5CB-cell with the initial instant temperature deviation from the ambient temperature $\Delta T_{\max} = 5^\circ$C. During the first 10 ms the temperature relaxes fast, followed by slower relaxation thereafter. Even after 100 milliseconds the temperature remains $\Delta T \sim 0.15^\circ$C.

Numerical calculations of heating as cumulative action of many, 10-Hz repetition-rate pulses yield results presented in Fig. 10 for $\Delta T_{\max} = 10^\circ$C (solid curve) and $\Delta T_{\max} = 5^\circ$C (dotted curve). After 60 pulses ($\sim$6 s of irradiation) the temperature in the center of the LC-cell increased by $\Delta T \sim 5^\circ$C for $\Delta T_{\max} = 10^\circ$C, and $\Delta T \sim 4.5^\circ$C for $\Delta T_{\max} = 5^\circ$C. The slopes of the curves increase faster for the first 15–20 pulses, and for $\Delta T_{\max} = 5^\circ$C, ΔT is close to the temperature saturation value at the end of the sequence.

Evaluation of the phase shift caused in a laser beam by this temperature increase gives $\Delta\psi = 2\pi\,\Delta nL/\lambda$, where L is the LC-layer thickness, and $\Delta n = \Delta T \mathrm{d}n/\mathrm{d}T$. The number of rings as a result of self-phase modulation in space on the transverse profile of a beam is equal to $N = \Delta\psi/2\pi = \Delta TL(\mathrm{d}n/\mathrm{d}T)/\lambda$. For 5CB in the region from 26°C to 31°C $\mathrm{d}n/\mathrm{d}T$ is $\sim 2.5 \times 10^{-3}$ grad^{-1} for $\lambda = 0.532$ μm, $L = 125$ μm, and $\Delta T \sim 5^\circ$C, $N = 3$. A temperature increase after single pulse irradiation results in no diffraction rings in the beam. Only the cumulative action of many pulses approaching a steady-state value yields a stable spatial self-phase modulation elliptical ring pattern as displayed in Figs. 7 and 8. It should be noted

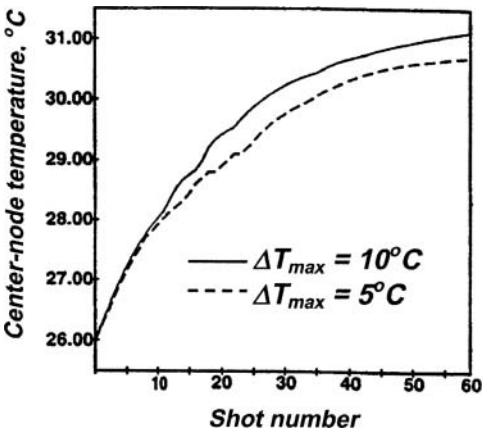

Figure 10. Numerical modeling of the heat diffusion: center-node temperature versus the number of pulses.

that some cumulative effects in LC nonlinearities at low pulse repetition rates were also reported in paper [69].

The observation of the effect only for incident polarization parallel to the LC-director is explained by two-photon absorption dichroism, and more effective LC heating by "parallel" polarization light, and approximately twice larger absolute value of dn/dT for "parallel" polarization in comparison with "perpendicular" polarization. The ellipticity of the ring patterns can be explained by the anisotropy of the thermal diffusion constant, which has for 5CB a $\sim$1.6 times larger value along the long molecular axis than perpendicular to it.

1.3. Feedback-Free Pattern Formation from Dye-Doped Liquid Crystals Under Nanosecond Laser Irradiation

In this chapter, I will describe some experimental results on high-definition patterns observed under 10-Hz-pulse-repetition-rate, nanosecond laser irradiation of highly absorbing planar-nematic LC layers doped with dichroic dye. The patterns were observed at incident intensities I $\sim$5–10 MW/cm^2 in a single beam and *without any feedback involved*. An incident polarization parallel to the nematic director was used. Under periodic pulsed laser irradiation, far-field beam patterns at the output of a dye-doped LC layer changed kaleidoscopically from rings and stripes to multiple hexagons. This pattern-formation regime had a buildup time of several seconds to minutes.

1.3.1. Experimental Setup and Cell Preparation. A 0.532-μm laser beam with a pulse duration of $\sim$20–26 ns and pulse repetition rate 10 Hz was focused by a 24-cm-focal-length lens into the dye-doped, planar-aligned nematic LC cell. The incident polarization was parallel to the orientation of the LC molecular director. The beam diameter in the focus was $\sim$150 μm at the 1/e level [70]. The far-field patterns were recorded from a screen by a video camera onto magnetic tape from which the spatial intensity distribution for each pulse was digitized afterwards.

The nematic LC mixture E7 doped with the dichroic azodye "Oil Red O" with a 1.5% weight-concentration was used for filling the LC cells. E7 was supplied by EM-Industries; Oil Red O was supplied by Sigma-Aldrich. Planar-aligned nematic LC-layers were prepared

using buffing techniques on Nylon 6/6 alignment layers on Soda-Lime-glass plates of size 2.5 cm × 2.5 cm × 0.3 cm. Glass-bead-spacers mixed with an UV-epoxy provided cell thicknesses between 10 and 20 μm. Coating the substrates by Nylon 6/6, buffing, cell assembly, and filling the cells with LC were carried out in a clean room. UV-cured epoxy was used for sealing the cells. Cell transmittance at low incident intensities was $\sim 1\%$ for an incident polarization parallel to the nematic director, and $\sim$10–15% for the perpendicular polarization.

1.3.2. Pattern Formation Experiments. At incident intensities $I \sim$1–5 MW/cm^2 several phenomena were observed during repetitive illumination of LC-cells by a focused laser beam with 10-Hz pulse-repetition rate, for time periods of *several seconds* to *several minutes*. These phenomena include the following [71]:

- A polarization component *perpendicular* to the nematic director appeared after the beam passed through the nematic layer. Simultaneously, a several-fold increase in cell transmission was observed.
- Following that, *stable* far-field patterns appeared in the beam cross-section, possibly as the result of heat-flow [72,73] and/or flow-reorientational [73–77] birefringence (Fig. 11):
  (1) The *perpendicular* polarization component (Fig. 11(b)) took on the far-field form of an optical four-leaf clover (Maltese-like cross). The bright axes of the cross were oriented at 45° to the incident polarization;
  (2) The incident, *parallel* polarization component evolved into the far-field pattern in the form of a ring with a bright spot inside (Fig. 11(c));
- *Stable* patterns existed for more than one hour of irradiation, but disappeared after switching the laser to a 5-Hz repetition rate.

At the higher-incident-intensities regime ($I \sim$5–10 MW/cm^2), a new kind of high-definition patterns developed with a buildup time of several seconds to minutes and only for the polarization component *parallel* to the nematic director. Figure 12 shows the beam cross-sections of the two spatially separated polarization components both incident and induced (using a Glan-prism) overlapping in the center. The left side of the images depicts *the parallel-polarization* (incident) component; the right side—*the perpendicular-polarization* (induced) component. The optical four-leaf-clover of the *perpendicular-polarization* component (Fig. 11(b)) almost always became smeared into a random speckle pattern with a bright spot in the center (see the right side of the images). At the same time, *the parallel-polarization* component developed a high-definition pattern that kaleidoscopically changed from pulse to pulse from multiple hexagons (Fig. 12(a)), stripes (Fig. 12(b)), to rings (Fig. 12(c)) (see left side of the Fig. 12 images). The patterns disappeared after switching the laser to 5-Hz repetition rate. More details will be published elsewhere.

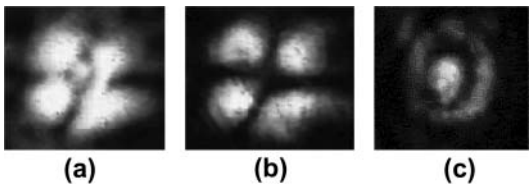

Figure 11. Far-field spatial patterns at low incident intensities: (a) no polarizer; (b) perpendicular-polarization (induced) component; (c) parallel (incident) polarization component.

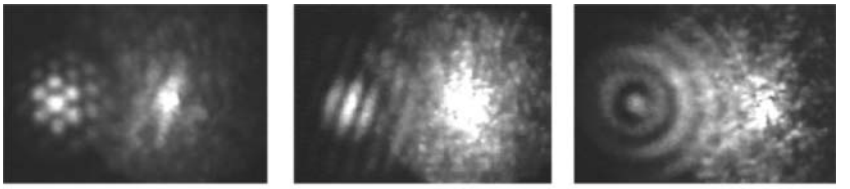

Figure 12. Representative selection of far-field spatial patterns at incident intensities of ∼5–10 MW/cm^2 for the polarization component parallel to the director (left side of each image) and for the induced, perpendicular polarization component (right side of each image). A Glan prism was used to separate the two polarizations.

Examination of the LC cells by optical polarizing microscopy after laser action showed no changes in planar alignment in most samples. However, in some samples, one, two, or three spots with destroyed alignment were seen very clearly. The dimensions of these spots were ∼12–30 μm with ∼50–90 μm distance between them.

Near-field images of the laser-beam cross-section during the pulsed laser action showed kaleidoscopic changes from one to two and three spots patterns with dimensions ∼5–15 μm and distance between spots ∼35–70 μm.

The observation of high-definition hexagonal/stripes/rings patterns only for the "parallel" polarization component can be explained by the highly dichroic dye used for this experiment: cell transmittance was an order of magnitude higher for the "perpendicular" polarization component than for the "parallel" polarization component. Hexagonal/stripes/rings patterns' low contrast makes them invisible for the "perpendicular" polarization component. Only a four-leaf-clover pattern can be seen in this component because of its existence's connection with another mechanism—the aberrations of the laser beam in heat-flow and/or flow-reorientational birefringent media.

We explain the observed hexagonal/stripes/rings patterns in the far-field by the diffraction of the laser beam on light-induced one/two/three or more several-micron-size "drops" with absorption and/or refraction properties different from the surrounding material. The patterns' ring structure can be attributed to the diffraction of laser light at the sharp boundary of the "drops". The variation in the "drop" numbers in the focal region, their size, the distance between them, and the gradient of transmittance inside the drop define the enormous variety of patterns we observed. A possible mechanism contributing to the creation of such "drops" is the instabilities in the presence of the Soret (thermal diffusion) effect, including phase separation of the dye from the liquid crystal. Phase separation of the dye from liquid crystal was also observed in Ref. 78 under cw-irradiation of a dye-doped liquid crystal.

2. Liquid Crystals at the Single-Photon Level And Under Near-Field Optical Microscopy

This chapter describes a new application for LCs—quantum information technology. A single-photon source (SPS) with definite polarization that efficiently produces photons exhibiting antibunching (separation of all photons in time) is a pivotal hardware element in absolutely secure quantum communication. For *single* photons, the second order correlation function $g^{(2)}(\tau) = \frac{<I(t)I(t+\tau)>}{<I(t)>^2}$ should have a minimum at $\tau = 0$ (in an ideal case $g^{(2)}(0) = 0$), indicating the absence of pairs, i.e., antibunching [79]. Here I is intensity. The critical issue in producing single photons exhibiting antibunching is the very low concentration of

photon emitters dispersed in a host, such that, within an excitation-laser focal spot, only one emitter becomes excited which will emit only one photon at a time, because of its finite fluorescence lifetime.

In the BB84 quantum key distribution protocol, the transmitter (Alice) and receiver (Bob) employ the linear and circular polarization states of single photons. The linear and circular polarization bases can be used to provide two different quantum level representations of zero and one. So a desirable feature for a SPS is definite photon polarization, since, if the photon has unknown polarization, filtering it through a polarizer to produce the desired polarization for quantum key distribution will reduce by half the efficiency of a quantum cryptography system. In another implementation, a SPS becomes the key hardware element for quantum computers with linear optical elements and photodetectors [80].

In this chapter, experimental results of *room temperature*, robust SPSs with definite polarization using *single*-emitter fluorescence in either *cholesteric* or *nematic* LC hosts are discussed [17–20,81–83]. A desirable polarization state (either circular with definite handedness or linear with definite direction) of a fluorescence of the emitter in a LC host can be produced either by providing a chiral microcavity environment of CLC or by aligning emitters' dipole moments in a definite direction in a nematic LC. SPSs based on single emitters in LCs are the room-temperature alternatives to cryogenic SPSs based on semiconductor heterostructured quantum dots in microcavities prepared by molecular beam epitaxy (MBE), see review [84]. Definite linear polarization of single photons from heterostructured quantum dots both in elliptical pillar microcavities, and in a 2-D photonic crystal, was reported for resonance wavelength at *cryogenic* temperatures. In difference to expensive MBE, well developed LC alignment technology is relatively easy and fast. Different types of single emitters can be easily dissolved or dispersed both in monomeric (fluid-like) or oligomeric (solid) LCs. In addition to emitter alignment and the possibility of fabrication of photonic-bandgap structures from LCs, LC technology has another advantage. Special treatment of LCs (oxygen depletion) can protect the emitters from bleaching [18,19]. In Ref. 18,19, we reported on a significant diminishing of dye bleaching by saturation of LC with helium. Another remarkable advantage of LCs, e.g., changing its properties with temperature or by external-field variation, can provide SPS tunability. As single emitters, we used nanocrystal quantum dots (NQD), single NV-color centers in nanodiamonds, and single dye molecules.

The structure of this chapter is as follows. Section 2.1 describes the results on antibunching and circular polarized fluorescence with desired handedness from colloidal semiconductor nanocrystal quantum dots (NQDs) embedded into planar-aligned CLC monomeric or oligomeric hosts. Some results on circularly polarized resonance of a CLC photonic bandgap microcavity *under cw-irradiation* are also briefly outlined. Section 2.2. is devoted to linearly polarized fluorescence with a definite polarization state from single dye molecules aligned in a glassy nematic LC oligomer. The last section 2.3. of this chapter describes near-field optical microscopy with simultaneous atomic force microscopy (AFM) of hexagonal arrays which I fabricated from glassy cholesteric oligomer.

2.1. Single-Photon Source with Definite Circular Polarization

It is well-known, that a planar-aligned CLC structure can be viewed as a 1-D photonic bandgap material, with a bandgap within which propagation of light is forbidden [85]. For emitters located within this structure, the spontaneous emission rate is suppressed within the spectral stopband and enhanced near the *band edge* [85]. CLC lasing experiments both

from the literature [85–90] and our own experiments on lasing in monomeric [91] and glassy oligomeric [92] CLCs confirmed that the best condition for coupling is when the dopant fluorescence maximum is at one of the band edges of the CLC selective transmission curve. For single-photon-source applications we used the same CLC hosts both monomeric and glassy oligomeric, but with dopant concentration of ∼1–10 nM.

Room-temperature SPSs based on colloidal nanocrystal quantum dots (NQD) fluorescence are very promising because of higher NQD photostability at room temperature than that of conventional dyes, and relatively high quantum yield (up to ∼100%). Electrically driven light emission from a single colloidal NQD at room temperature was obtained in Ref. 93, opening up the possibility for electrical pumping of a SPS on demand, based on colloidal NQDs.

Our SPSs are based on single colloidal CdSe (fluorescence wavelength λ_o ∼580 nm), CdSeTe (λ_o ∼700 nm) or CdSeTe (λ_o ∼790 nm) NQDs suspended in CLC hosts.

2.1.1. Experimental Setup for Antibunching and Circular Polarization Measurements. The experimental setup consists of a home-built, confocal fluorescence microscope based on a Nikon TE2000-U inverted microscope with several output ports. Figure 13 shows a photograph of this microscope. Detailed schematic of the experimental setup is provided in Refs. 20, 82, 83.

We excite our samples with 76-MHz repetition-rate, 6-ps pulse duration, 532-nm light from a Lynx mode-locked laser (Time-Bandwidth Products Inc.). In some experiments, we used a cw-532-nm, ion argon laser (514 nm) or He-Ne laser ($\lambda = 633$ nm). To obtain a diffraction-limited spot on the sample, the excitation beam is expanded and collimated by

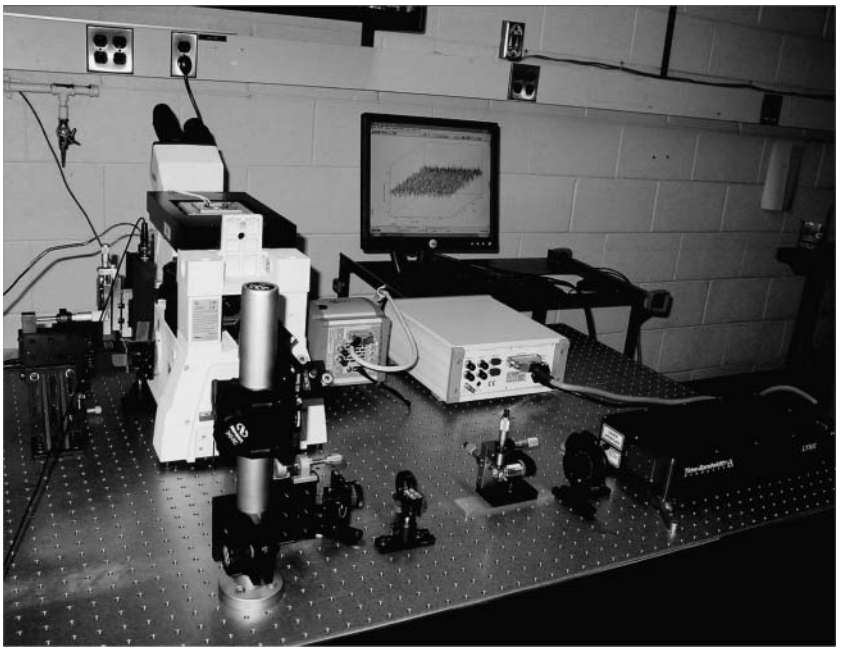

Figure 13. Picture of the experimental setup (a home-built confocal fluorescence microscope with the laser and the diagnostic tools shown).

a telescopic system with a spatial filter. The samples are placed in the focal plane of a 1.3-numerical aperture (NA), oil-immersion microscope objective used in confocal reflection mode. In focus, the intensities used are of the order of several kW/cm^2. Residual transmitted excitation light is removed by a dichroic mirror and a combination of two interference filters yielding a combined rejection of 9–11 orders of magnitude at the excitation wavelength. The sample's holder is attached to a piezoelectric, XY translation stage providing a raster scan of the sample through an area of up to 50 μm $\times$ 50 μm.

In the below described measurements, we used two output ports of this microscope. The first port contained a spectrometer [fiber-optical (Ocean Optics) with a several seconds accumulation time with background subtraction or SpectraPro2150i (Princeton Instruments) with an EM-CCD camera iXon DV887 (Andor Technologies)]. Circular polarization measurements were accomplished using an achromatic quarter-wave plate and linear polarizer.

Measurements of fluorescence antibunching were carried out using another port of the confocal fluorescence microscope by directing NQD fluorescence to a Hanbury Brown-Twiss interferometer. The interferometer consists of a beamsplitter, two single-photon avalanche photodiode modules (AQR-14, Perkin-Elmer), and a time-correlated single-photon counting card (TimeHarp 200, PicoQuant) with start and stop channels. To build a histogram of interphoton times, we used a 63 ns variable delay in the stop channel.

2.1.2. Chiral Microcavities Made of CLCs Doped with Single NQDs: Preparation and Characterization. For sample preparation we used monomeric mixtures of low-molecular-weight E7 nematic-LC blended with the chiral additive CB15. Both materials were supplied by EM Industries. We filtered E7 and CB15 to remove fluorescent contaminants.

After monomeric CLC preparation, a NQD solution in toluene was mixed with monomeric CLC and the solvent was evaporated. To work with the high-NA microscope objective, the cell was made using two microscope cover glass slips with $\sim$120 μm thickness. Planar alignment was achieved either using buffing with special tool for cover slips or through unidirectional mechanical motion between the two slides. For further details of CLC doping and sample preparation see [17–20,81–83].

Figure 14 shows selective-transmission curves of three monomeric (a) and (b), (c) and one oligomeric (d) planar-aligned CLC structures. To obtain these curves in the case of (a) and (b) CLC structures, we used an achromatic quarter waveplate to obtain circularly polarized incident light. For CLC structures (c) and (d), the measurements of selective transmission were carried out using unpolarized light. Figure 14 also shows the fluorescence spectra of the CdSe, CdSeTe and PbSe NQDs with the fluorescence peaks near 580 nm, 700 nm and 1.5 μm.

CdSe/ZnS core/shell and PbSe NQDs were synthesized by T. Krauss' group (University of Rochester). CdSeTe QDs were obtained commercially from Invitrogen.

2.1.3. Circular Polarized Fluorescence and Antibunching in a CLC Microcavity. Figure 15 (curves 1 and 2) show emission spectra for CdSe/ZnS NQDs in a CLC microcavity for right-handed (RH) and left-handed (LC) circular polarizations (CP). Selective transmission curve of a CLC structure is shown as well (curve 3). The degree of circular polarization is measured by the dissymmetry factor g_e:

$$g_e = 2(I_L - I_R)/(I_L + I_R), \tag{6}$$

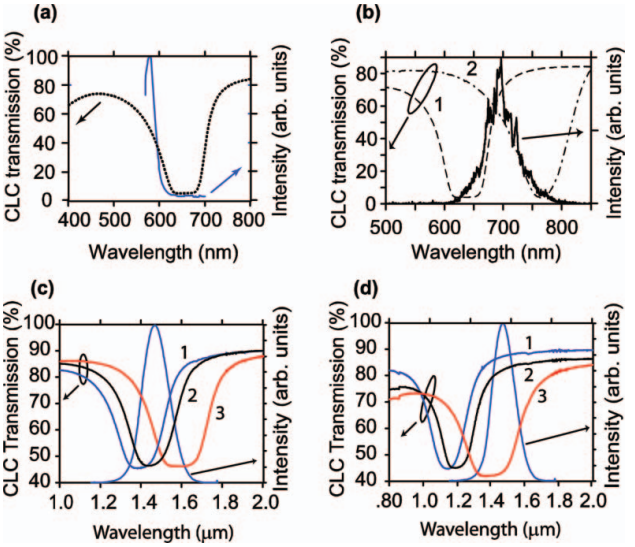

Figure 14. CLC photonic-bandgap selective transmission curves, using either *monomeric* or *oligomeric* CLC. Also shown are the NQD fluorescence spectra that these transmission curves were tuned to. In (a–b), the CLC transmission was measured with right-handed circularly-polarized light; in (c–d), unpolarized light was used. (a) CdSe NQDs ($\lambda_o = 580$ nm). The weight concentrations of chiral additive CB15 in the CB15/E7 mixture is $c_m = 36.6\%$. (b) CdSeTe NQDs ($\lambda_o = 700$ nm). Here, $c_m = 36.0\%$ (curve 1), and $c_m = 29\%$ (curve 2). (c) PbSe NQDs ($\lambda_o = 1.5$ μm). Here, $c_m = 16.3\%$ (curve 1), $c_m = 16.0\%$ (curve 2), and $c_m = 14.4\%$ (curve 3). (d) PbSe NQDs. The ratio of Wacker oligomeric powders with $\lambda_o = 1.17$ μm and $\lambda_o = 2.15$ μm were, $r_o = 1{:}0$ (curve 1), 1:0.24 (curve 2), and 1:1 (curve 3).

where I_L and I_R are the intensities of LH and RH CPs. At 580 nm, $g_e = -1.6$ [82,83]. For unpolarized light $g_e = 0$. Using another type of CLC, e.g., Wacker CLC oligomers, left-handed circular polarization of single photons can be obtained [20].

Figure 16(a) shows a confocal-fluorescence-microscope image of several NQDs in a monomeric CLC. For antibunching measurements, we focused a laser beam on a single

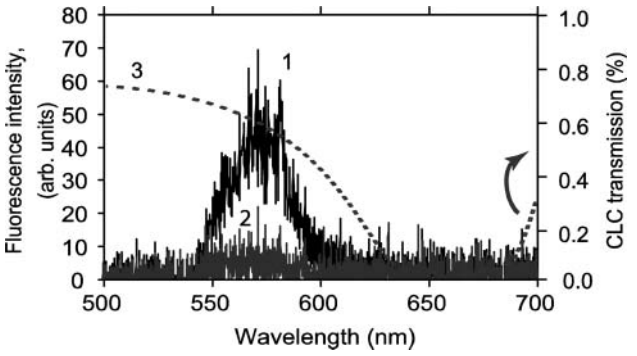

Figure 15. Right-handed, circularly-polarized fluorescence of CdSe NQDs in a CLC microcavity. Curve 1: RHCP fluorescence spectrum. Curve 2: LHCP fluorescence spectrum. Curve 3: Transmission curve of monomeric CLC (E7 + CB15) host for RHCP light.

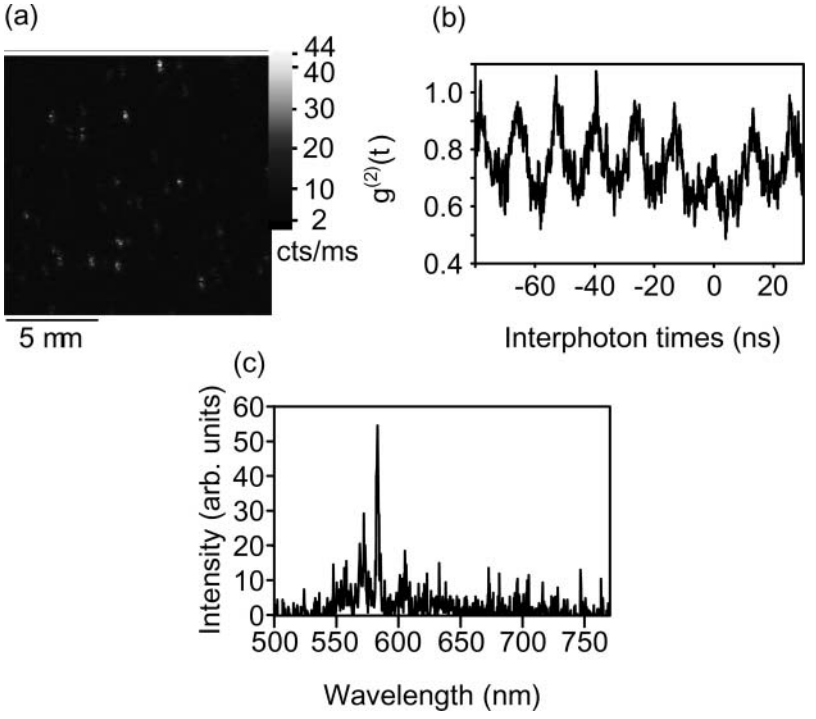

Figure 16. Antibunched fluorescence of CdSe NQDs ($\lambda_o = 580$ nm) in a monomeric CLC microcavity. (a) Confocal microscopy image of fluorescence from single CdSe NQDs. (b) Antibunched coincidence-count histogram obtained from illuminating a single CdSe NQD. (c) Fluorescence spectrum of the undoped CLC host (mixture of nematic E7 and chiral additive CB15).

NQD and measured the fluoresced photon statistics under saturation conditions. A 532-nm laser with 6-ps pulse duration and 76-MHz pulse repetition rate was used in this experiment. Figure 16(b) presents the $g^{(2)}(t)$ histogram at different interphoton times t. One sees that the peak at zero interphoton time is clearly smaller than any of the other peaks, which shows an antibunching property [$g^{(2)}(0) = 0.76 \pm 0.04$]. This antibunching histogram can be improved by using NQDs which fluoresce outside the fluorescence spectrum of the CLC shown in Fig. 16(c). The spectral peaks which were observed in the CLC cavity without NQDs can be attributed to Raman scattering in the CLC. It is not a microcavity effect, because we observed the same features from unaligned CLC without a microcavity.

In order to avoid the CLC host fluorescence, we selected CdSeTe NQDs with $\lambda_o = 700$ nm and doped them into the CLC host with the stop band shown in Fig. 14(b) (curve 1). When illuminating a single NQD, we obtained antibunching with $g^{(2)}(0) = 0.001 \pm 0.03$ [Fig. 17(a)]. The spontaneous decay rate for these NQDs (20 MHz) is less than the laser excitation rate (76MHz), so we cannot observe fluorescence excited by separate laser pulses as in Fig. 16(b).

Figure 17(b) shows the normalized coincidence histogram for fluorescence of CdSeTe NQD doped in the same CLC host (Fig. 14(b), curve 1), illuminated with cw, 532-nm light. We observed antibunched fluorescence with $g^{(2)}(0) = 0.11 \pm 0.06$.

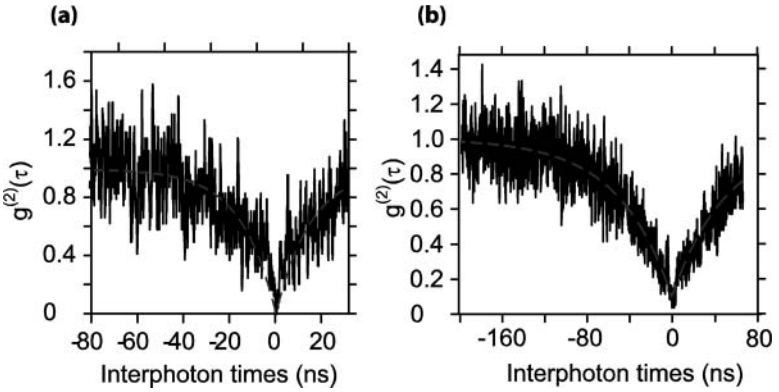

Figure 17. Antibunched fluorescence of CdSeTe NQDs ($\lambda_o = 700$ nm) in a monomeric CLC host using pulsed and cw excitation. Normalized coincidence histograms showing fluorescence antibunching of CdSeTe NQDs ($\lambda_o = 700$ nm) in a CLC host under: (a) 532-nm, pulsed excitation (see explanation in text), and (b) 532-nm, cw excitation.

Our results show that using LCs as the host, to obtain better fluorescence antibunching of single emitters we should select emitters with fluorescence wavelength outside the host background, or use an upconversion excitation process to excite single emitters.

2.1.4. Circular Polarized Microcavity Resonances in Chiral Cholesteric Liquid Crystal Microcavity Under Cw-Irradiation. We also placed nanodiamonds with N-vacancy (NV) color centers with $\lambda_o = 650$ nm inside a monomeric (E7 and CB15) CLC host with a stop band centered at 725 nm [20]. Cw, 514-nm excitation was used. These nanodiamonds were purchased from Microdiamant AG, Switzerland. They are agglomerate free, and ∼30–50 nm in diameter. Fig. 18(a) shows fluorescence antibunching from this color center. The fitted value for $g^{(2)}(0)$ is 0.74 ± 0.08. The spectrum of the nanodiamond NV color centers is shown in Fig. 18(b). It should be noted that a monomeric CLC host fluoresces in a spectral

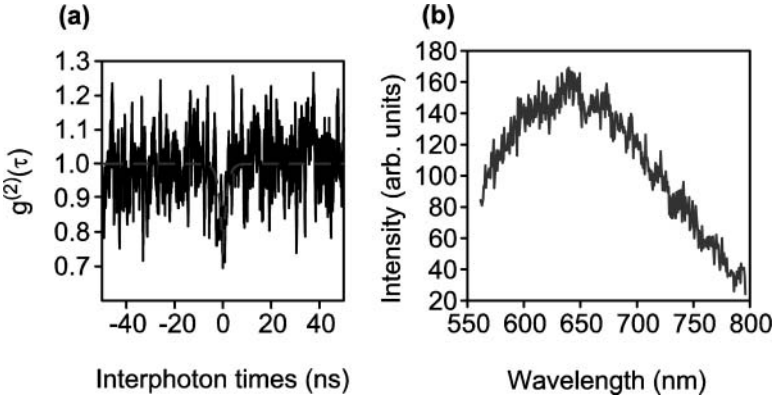

Figure 18. (a) Antibunched fluorescence from nanodiamond N-vacancy color centers embedded in a monomeric CLC host. The raw data are plotted in black. The dashes denote the fit to the raw data, (b) Fluorescence spectrum of the nanodiamond N-vacancy color centers in a monomeric CLC host. 514-nm, cw excitation was used. See Ref. [20].

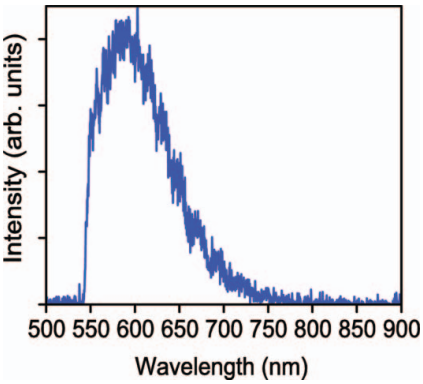

Figure 19. Spectrum of undoped, Wacker glassy-oligomer CLC. The abrupt transition at the left edge of the spectrum is from the interference filter used to block the 532-nm excitation.

region of this color center (Fig. 16(c)). To reduce $g^{(2)}(0)$, different types of color centers should be used, e.g., Ni-related color centers with emission wavelength near 800 nm.

A glassy Wacker oligomeric CLC structure (Fig. 19) with a photonic stop band centered at 750 nm was prepared (Fig. 20(a)). This structure was illuminated with cw, 532-nm laser light. We doped the CLC with a low concentration of nanodiamonds with NV color centers. Although we were not able to record NV-color center fluorescence spectrum in this sample, we observed a resonance at the left band-edge of the photonic stop band. Fig. 20(a) shows this resonance, centered at 620 nm, with a FWHM of ∼3 nm (the quality factor is Q ∼250). The resonance was stable. Another remarkable property of the resonance is circular polarization, as shown in Fig. 20(b). We believe it results from microcavity enhancement of a glassy CLC fluorescence in this spectral region (see Fig. 19).

We also observed circularly polarized resonance of the NQD fluorescence at 833 nm on the band edge of a CLC photonic band gap structure [94–96] within a FWHM of 16 nm.

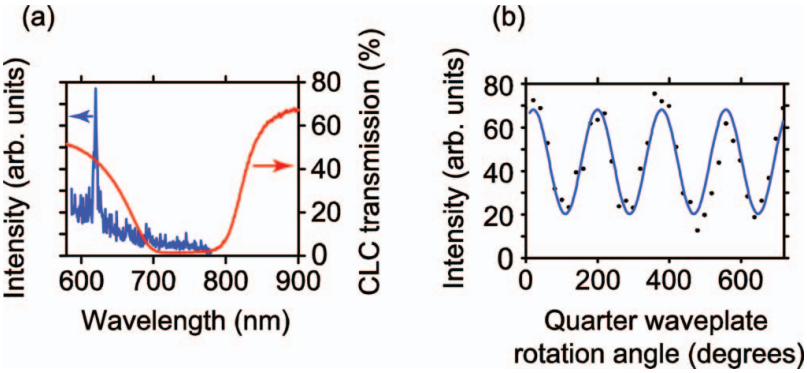

Figure 20. Circularly-polarized fluorescence resonance of a glassy CLC microcavity. (a) Selective transmission of circularly-polarized light through a glassy oligomeric CLC microcavity with a photonic stop band centered at 750 nm, and fluorescence spectrum of this sample with a resonance at 620 nm. (b) Dependence of the resonance-peak intensity on rotation angle of a quarter-wave plate with a fixed linear polarizer, showing circular polarization. The curve is a sinusoidal fit to the data points (black dots).

2.2. Single-Photon Source with Definite Linear Polarization

The second SPS is based on single dye molecule fluorescence (DiI or terrylene) from a chromophore suspended in planar-aligned *nematic* LCs. Linearly polarized single-photon emission with definite polarization was obtained from single molecules of DiI dye doped into a planar-aligned glassy nematic LC oligomer [17,81]. This oligomer [17,81] was synthesized by the S.-H. Chen's group. An oligomer solution with a 1% concentration by weight in chloroform with 10^{-8} M concentration of the dye in chloroform was prepared. After spin-coating the dye-doped oligomer solution onto the photo-aligned Staralign-coated slip, the sample was heated on a hotplate above transition to the nematic state ($\sim 80^{\circ}$C) for 30 minutes and slowly cooled to the glassy state with preserved nematic order [17,81].

For single-molecule fluorescence imaging we used a Witec alpha-SNOM microscope in confocal transmission mode (Fig. 21). A detailed description of the setup is presented in Refs. 17 and 81. Images of single-molecule fluorescence for polarization components perpendicular (left) and parallel (center) to the LC alignment direction, under 532-nm, cw-excitation are presented in Refs. 17 and 81. These two polarization components in the plane of the sample have been separated with a polarizing beamsplitter cube. The single-molecule-fluorescence signal exceeded the background by up to 15 times. Processing of these images with background subtraction shows that from a total of 38 molecules, 31 molecules have a negative value of the degree of linear polarization

$$\rho = (I_{\text{par}} - I_{\text{perp}})/(I_{\text{par}} + I_{\text{perp}}), \tag{7}$$

where I_{par} and I_{perp} are fluorescence intensities for polarization components parallel and perpendicular to the alignment direction. The histogram in Fig. 22 shows a distribution of these molecules with different ρ. The same sign of ρ was obtained in spectrofluorimeter

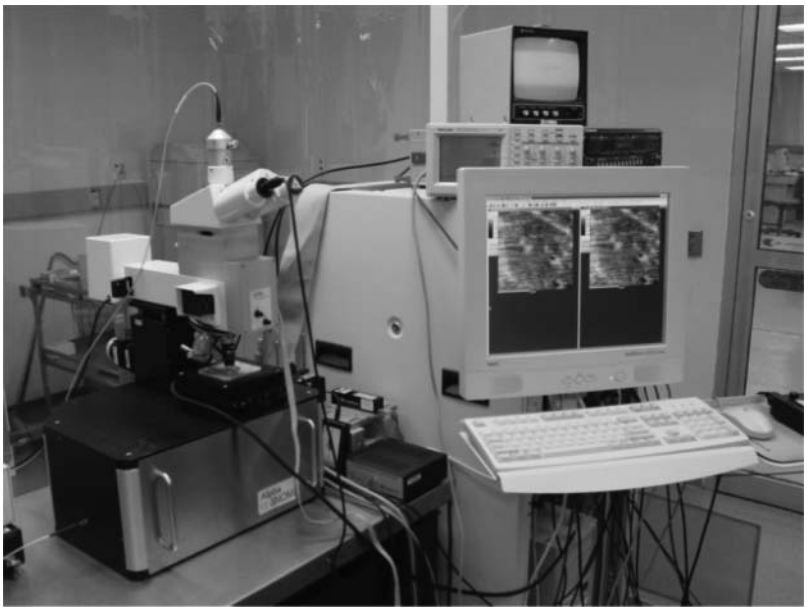

Figure 21. The Alpha-SNOM microscope used in some experiments. It comprises a confocal fluorescence and a near-field microscope, as well as an AFM, all on one platform.

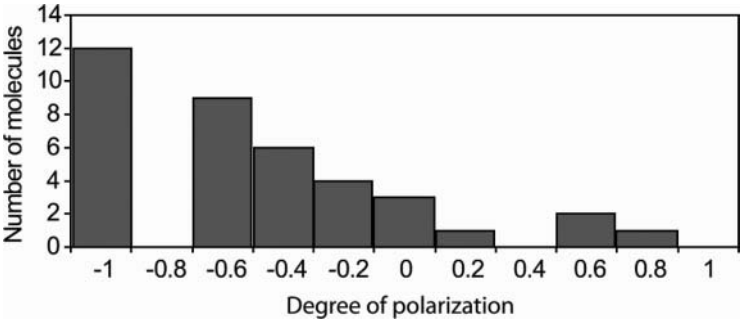

Figure 22. The histogram of the degree of polarization of 38 molecules of DiI dye in a planar-aligned, glassy nematic LC host. In difference with the symmetrical histogram for random orientation of DiI dye molecular dipoles (see discussion in Ref. [81]), this histogram is assymmetrical.

measurements from a sample with a high concentration of the same dye in a planar-aligned, nematic LC layer. This predominance of "perpendicular" polarization in Fig. 22 can be explained by DiI dye molecular structure [17,81]. The two alkyl chains likely orient themselves parallel to the rod-like LC molecules, but the emitting/absorbing dipoles which are parallel to the bridge (perpendicular to the alkyl chains) will be directed perpendicular to the LC alignment direction.

Figure 23 presents the results of another experiment [20] in which we collected fluorescence from several single molecules of DiI dye doped in nematic LC E7 (100 nM concentration). The LC was aligned by the method of unidirectional mechanical motion between two cover-glass slips. A spectrometer, SpectraPro2150i (Princeton Instruments), and an EM-CCD camera (Andor Technologies) were used to observe DiI fluorescence spectra for two linear polarizations. Figure 23(a) shows the change in fluorescence intensity of DiI molecules in E7 as the linearly-polarized excitation light is rotated through 360°, relative to the perpendicular direction. It can be seen that the maximum fluorescence occurs when the DiI is excited along the direction perpendicular to the alignment. Figure 23(b)

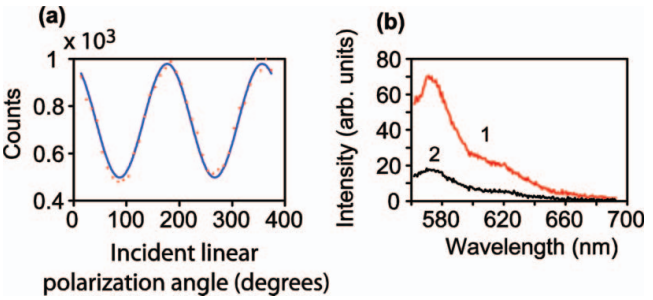

Figure 23. Linearly-polarized fluorescence of DiI dye molecules doped into the nematic liquid crystal E7. (a) Dependence of DiI fluorescence polarization on excitation polarization. The polarization angle shown is relative to the direction perpendicular to the liquid crystal alignment. Dots: experimental data, curve: sinusoidal fit to the data. (b) Fluorescence spectra for the measurement of the degree of polarization of DiI fluorescence with excitation perpendicular to the alignment direction. Curves 1 and 2 denote DiI fluorescence spectra polarized along the direction perpendicular and parallel to the alignment, respectively (see Ref. [20]).

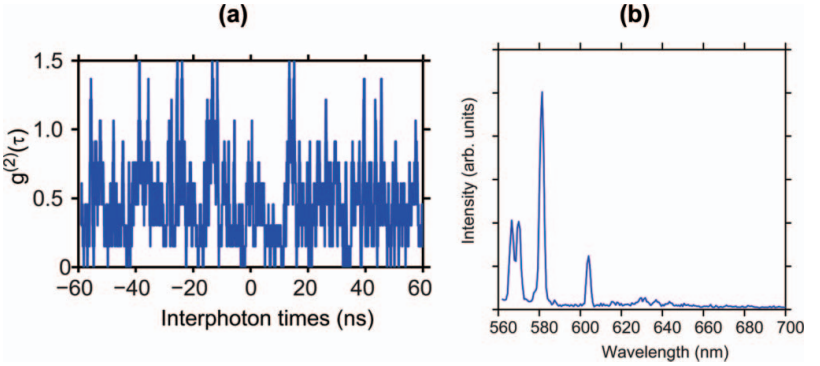

Figure 24. (a) Fluorescence antibunching of DiI in nematic LC E7; (b) fluorescence spectrum of the nematic LC E7, under 532-nm excitation (see Ref. [20]).

shows fluorescence spectra for perpendicular polarization (curve 1) and parallel (curve 2) polarization when the excitation light is polarized perpendicular to the alignment direction. Here the degree of polarization is $\rho = -0.58 \pm 0.03$. As the excitation-light polarization is rotated away from the perpendicular direction, the degree of polarization decreases.

Figure 24(a) shows a fluorescence-antibunching histogram for DiI dye in E7 (1-nM concentration) with $g^{(2)}(0) = 0.77 \pm 0.10$ [20]. The relatively high value of $g^{(2)}(0)$ can be attributed to the fact that the E7 fluorescence spectrum [Fig. 24(b)] overlaps that of DiI [Fig. 23(b)]. The DiI molecules were excited with pulsed, 532 nm light. Because the fluorescence lifetime of DiI in E7 is ∼1.8 ns, which is shorter than 13.3-ns distance between excitation laser pulses, periodic peaks in the $g^{(2)}$(t) histogram are observed.

2.3. Near-Field Optical Microscopy of Fabricated Hexagonal Arrays in a Cholesteric Liquid Crystal Oligomer

Here we report results on 2-D, hexagonal ordering in oligomeric CLC films during solvent evaporation from the substrate in a specific range of oligomer concentrations [97]. Both near-field optical microscopy and simultaneous AFM showed the existence of such ordering with a periodicity of ∼0.5–0.8 μm. The combined action of convection and water droplet condensation during the evaporative cooling are the suggested mechanisms for the observed hexagonal patterns.

With further development of this technology, our results are promising for the fabrication of 2-D and 3-D photonic crystals for both visible and near-IR spectral regions by this relatively simple method (see, for instance, Ref. 98). Created in this manner, photonic-bandgap materials doped with appropriate chromophore can be used for fluorescence control in photonic devices, for instance, in efficient single-photon sources and oligomeric LC lasers.

2.3.1. Preparation of Oligomeric CLC Films. For our experiments, we used Wacker oligomer LC-4627 with maximum selective reflection wavelength $\lambda_o = 2.2$ μm. The oligomer powder was dissolved either in chlorobenzene or in methylene chloride with approximately 8.4–15.6% concentration of Wacker oligomer by weight. Lower concentration of oligomer with lower solution viscosity did not provide for the film self-assembly reported in the present paper. We prepared oligomer thin films on clean Corning cover glass slips

(25 mm × 25 mm, 170 μm thickness) by holding the slip at close to 90^o degree angle and dripping the oligomer solution on to it. The solvent evaporated very quickly under the clean-air flow of the fume hood.

Optical-polarizing-microscope images of the samples prepared from solutions with different concentrations of the oligomer reveal the appearance of domain structure where each cell is surrounded by boundaries [97]. The widths of the domains are approximately 50–100 μm. Their shapes vary from circles and ovals to long stripes with near 1-mm-lengths [97]. Similar cell domains have been observed in Ref. 99 in the process of evaporation of solvent in which both nematic and polymer were dissolved.

To define the thickness of the film, an AFM of a razor-blade-cut of the sample was made. The film prepared from a solution with the lowest oligomer concentration (∼8.4% weight concentration) showed a thickness of 65 nm in an area free of defects.

2.3.2. Near-Field Optical Microscopy and AFM of Defects in Films of Wacker CLC Oligomers. A cantilever SNOM (WiTec alpha-SNOM) (Fig. 21) in "tapping" mode with ∼100-nm tip aperture enables both near-field optical microscopy and simultaneous topographic imaging. Figure 25 shows scanning near-field optical microscopy images (left) and AFM images (right) of hexagonal ordering in defects (boundaries of macroscopic domains described in section 2.3.1) of the prepared oligomer layer. The bottom images (both near-field microscopy and AFM) were taken simultaneously during the scan.

Another set of images of a different area with hexagonal ordering (Fig. 26) represents the AFM image (left) and near-field images of this area for two different polarizations.

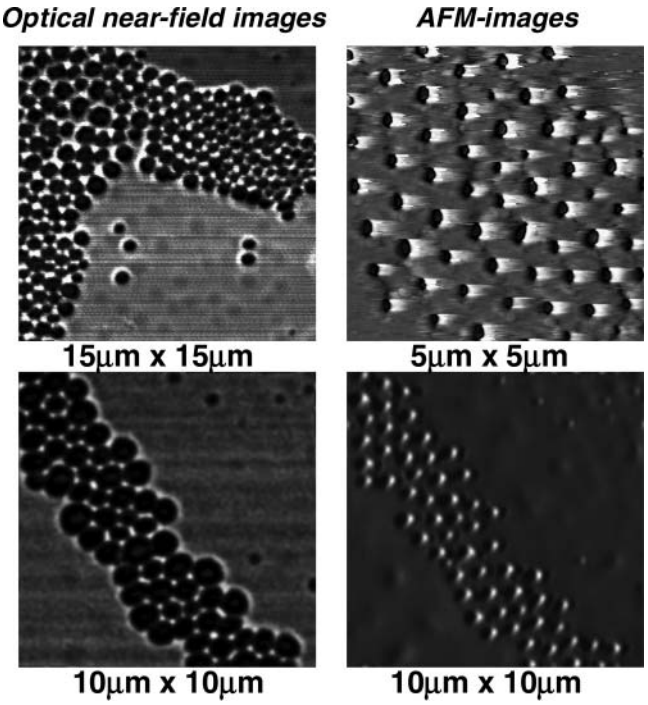

Figure 25. Near-field optical microscopy (left) and AFM (right) images of Wacker oligomer film defects with hexagonally ordered arrays. Bottom images were taken simultaneously.

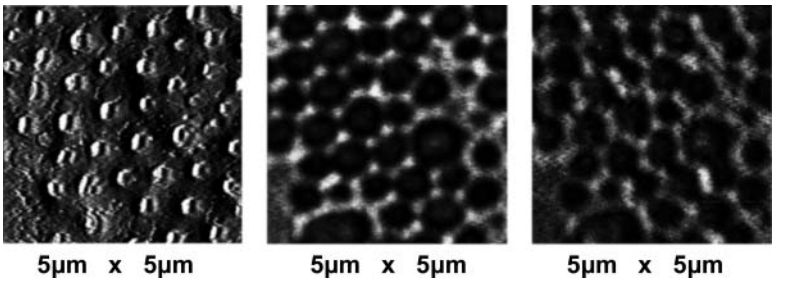

Figure 26. AFM (left) and near-field optical microscopy images (center and right) for two different polarizations of the laser beam showing the hexagonal ordering of Wacker oligomer film defects.

Explaining such arrays in our experiments, we suggest a mechanism which has been detailed in Ref. 98. Cooling by the evaporating solvent leads ambient moisture to condense on the hydrophobic mixture. Water droplets segregate and entrap into these self-assembling, hexagonally-ordered patterns [98,100]. Within minutes, the system returns to equilibrium with the water evaporated from the cavities leaving the air bubbles on the film surface.

Summary

An overview of some experiments and new applications of liquid crystals under two "extreme" levels of incident light powers are presented. In many such applications for better device performance, "as received" liquid crystals materials must be purified and degassed. Several effects under high-power, nanosecond laser irradiation are outlined: (1) athermal helical pitch dilation and unwinding of cholesteric mirrors by the field of a light wave; (2) dependence of thermal-density refractive nonlinearity on the geometry of irradiation; (3) the first observation of thermal lens effects in liquid crystals under several-nanosecond, low-pulse-repetition rate (2–10 Hz) laser irradiation in the presence of two-photon absorption; (4) feedback-free pattern kaleidoscope in dye-doped, highly absorbing liquid crystals.

At the single-photon level, definite linear and circular polarizations of single (anti-bunched) photons were obtained using single-emitter fluorescence in planar-aligned nematic and cholesteric hosts. Circular-polarized, cholesteric microcavity resonances were also observed under cw-excitation. These results are important for creation of room-temperature, single-photon sources, key devices for absolutely secure quantum communication. In addition, using near-field optical microscopy and AFM, 2D-hexagonal arrays made of cholesteric oligomers were investigated. With development of this technology, similar arrays can be used for fluorescence control of single emitters for single-photon source applications as well as for development of new compact microlasers.

Acknowledgments

The author acknowledge the support by the U.S. Army Research Office Award DAAD19-02-1-0285, National Science Foundation Awards ECS-0420888, DUE-0633621, DUE-0920500, and NASA NNX11AM82H Award. Research carried out in Russia was supported by the International Science Foundation Long-Term Award, Russian Government and Russian Foundation for Basic Research Awards.

Some figures were reproduced from Ref. 28 with permission from World Scientific Publishing Co. Pte. Ltd.

The author thanks A.W. Schmid, S.V. Belyaev, V.F. Zolin, Ch.M. Briskina, V.M. Markushev, P. Palffy Muhoray, T. Kosa, B. Taheri, R. W. Boyd and his group members, L.J. Bissell, K. Marshal, L. Novotny and his group members, A. Lieb, J. Winkler, C.R. Stroud, S.-H. Chen and his group members, T. Krauss and his group members for help and/or support. These experiments were carried out in three institutions: the Institute of Radio Engineering and Electronics of the Russian Academy of Sciences, Moscow, Russia; the Liquid Crystal Institute (Kent State University), USA; the Institute of Optics, University of Rochester, USA. Some experiments were carried out at the liquid-crystal clean room and nanometrology facilities at the Laboratory for Laser Energetics, University of Rochester. The paper title was suggested jointly with N. Tabiryan.

References

[1] Jacobs, S. D., Cerqua, K. A., Marshal, K. L., Schmid, A. W., Guardalben, M. J., & Skerrett, K. J. (1988). *JOSA. B*, *5*, 1962.
[2] Schmid, A., Papernov, S., Li, Z.-W., Marshal, K., Gunderman, T., Lee, J.-C., Guardalben, M. J., & Jacobs, S. D. (1991). *Mol. Cryst. Liq. Cryst.*, *207*, 33.
[3] Jacobs, S. D., Marshal, K. L., & Schmid, A. (1995). In: M. J. Weber (Ed.), *Handbook of Laser Science and Technology, Supplement 2: Optical Materials*, CRC Press: Boca Raton, FL, pp. 509–577.
[4] Lukishova, S. G., Senatsky, Y. V., Bykovsky, N. E., & Scheulin, A. S. (2009). In: S. G. Lukishova, R. W. Boyd, & Y.-R. Shen (Eds.), *Self-focusing: Past and Present. Fundamentals and Prospects*, Springer Series: Topics in Applied Physics, vol. 114, Springer: NY, Chapter 8, pp. 191–229.
[5] Lukishova, S. G., Pashinin, P. P., Batygov, S. Kh., Arkhangelskaya, V. A., Poletimov, A. E., Scheulin, A. S., & Terentiev, B. M. (1990). *Laser and Particle Beams*, *8*(N 1–2), 349.
[6] Gorshkov, B. V., Ivanchenko, V. K., Karpovich, V. K., Krasyuk, I. K., Lukishova, S. G., Margolin, D. M., Pashinin, P. P., Simun, E. A., Sokolov, V. A., Terekhov, V. D., & Chernysheva, L. V. (1985). *Kvantovaya Elektronika*, *12*, 1453; (1985). *Sov. J. Quant. Electron.*, *15*, 959.
[7] Lukishova, S. G., Minhuey-Mendez, N. R., & Tulajkova, T. V. (1994). *Kvantovaya Elektronika*, *21*, 126; (1994). *Quant. Electron.*, *24*, 117.
[8] Lukishova, S. G., Chetkin, S. A., Mettus, N. V., & Magulariya, E. A. (1996). *Kvantovaya Elektronika*, *23*, 1040; (1996). *Quant. Electron.*, *26*, 1014.
[9] Lukishova, S. G., Boyd, R. W., Shen, Y.-R. (2009). Preface. In: S. G. Lukishova, R. W. Boyd, & Y.-R. Shen (Eds.), *Self-focusing: Past and Present. Fundamentals and Prospects*, Springer Series: Topics in Applied Physics, vol. 114, Springer: NY, pp. V–XVIII.
[10] Lee, J.-C. Jacobs, S. D., Gunderman, T., Schmid, A., Kessler, T. J., & Skeldon, M. D. (1990). *Opt. Lett.*, *15*, 959.
[11] Lee, J.-C., Jacobs, S. D., & Gingold, R. J. (1987). *Proc. SPIE*, *824*, 7.
[12] Lee, J.-C., Jacobs, S. D., & Schmid, A. W. (1987). *Mol. Cryst. Liq. Cryst.*, *150b*, 617.
[13] Lee, J.-C., Schmid, A. W., & Jacobs, S. D. (1989). *Mol. Cryst. Liq. Cryst.*, *166*, 253.
[14] Lee, J.-C., & Jacobs, S. D. (1990). *J. Appl. Phys.*, *68*, 6523.
[15] Lee, J.-C., Kelly, J. H., Smith, D. L., & Jacobs, S. D. (1988). *IEEE J. Quant. Electron.*, *24*, 2238.
[16] Schmid, A. W. private communication.
[17] Lukishova, S. G., Schmid, A. W., Knox, R. P., Freivald, P., McNamara, A., Boyd, R. W., Stroud, C. R., Jr., & Marshall, K. L. (2006). *Molec. Cryst. Liq. Cryst.*, *454*, 1–14.
[18] Lukishova, S. G., Schmid, A. W., McNamara, A. J., Boyd, R. W., & Stroud, C. R. (2003). *IEEE J. Select. Top. Quantum Electron.*, *9*(6), 1512.
[19] Lukishova, S. G., Schmid, A. W., Supranowitz, Ch. M., Lippa, N., McNamara, A. J., Boyd, R. W., & Stroud, C. R., Jr. (2004). *J. Mod. Opt.*, *51*(9–10), 1535.

[20] Bissell, L. J. (2011). *Experimental Realization of Efficient, Room-Temperature Single-Photon Sources with Definite Circular and Linear Polarizations*, Ph.D. Thesis, University of Rochester, Rochester, NY.
[21] Winful, H. G. (1982). *Phys. Rev. Lett.*, *49*, 1179.
[22] Becker, R. S., Chakravorti, S., & Das, S. (1989). *J. Chem. Phys.*, *90*, 2802.
[23] Espinet, H., Lesieski, M., Ramsburg, M., & Jenkins, D. (1986). *J. Appl. Phys.*, *59*, 1386.
[24] Lukishova, S. G., Magulariya, E. A., & Lebedev, K. S. (1995). *Izvestiya Akademii Nauk Seriya Fizicheskaya*, *59*, 130; (1995). *Bulletin Russian Acad. Sci., Phys.*, *59*, 2086.
[25] Lukishova, S. G., Lebedev, K. S., Magulariya, E. A., Belyaev, S. V., Malimonenko, N. V., & Schmid, A. W. (1996). *JETP Lett.*, *63*, 423.
[26] Lukishova, S. G., Belyaev, S. V., Lebedev, K. S., Magulariya, E. A., Schmid, A. W., & Malimonenko, N. V. (1996). *Kvantovaya Elektronika*, *23*, 817; (1996). *Quantum Electron*., *26*, 796.
[27] Lukishova, S. G., Belyaev, S. V., Lebedev, K. S., Magulariya, E. A., Schmid, A. W., & Malimonenko, N. V. (1997). *Mol. Cryst. Liq. Cryst.*, *303*, 79.
[28] Lukishova, S. G. (2000). *J. Nonl. Opt. Phys. & Mater.*, *9*(N 3), 365.
[29] Grebe, D., Macdonald, R., & Eichler, H. J. (1996). *Mol. Cryst. Liq. Cryst.*, *282*, 309.
[30] Blinov, L. M., & Palto, S. P. (2009). *Liquid Crystals*, *36*, 1037.
[31] Gennes, P. G. de. (1974). *The Physics of Liquid Crystals*, Clarendon Press: Oxford.
[32] Blinov, L. M. (1983). *Electro-Optical and Magneto-Optical Properties of Liquid Crystals*, John Wiley & Sons: New York.
[33] Blinov, L. M., & Chigrinov, V. G. (1992). *Electrooptic Effects in Liquid Crystal Materials*, Springer Verlag: New York.
[34] Blinov, L. M., Belyaev, S. V., & Kisel, V. A. (1978). *Phys. Lett.*, *A 65*, 33.
[35] Belyaev, S. V., & Blinov, L. M. (1979). *JETP Lett.*, *30*, 99.
[36] Deeg, F. W., & Fayer, M. D. (1989). *J. Chem. Phys.*, *91*, 2269.
[37] Durbin, S. D., & Shen, Y. R. (1984). *Phys. Rev.*, *A 30*, 1419.
[38] Macdonald, R., & Eichler, H. E. (1995). *Appl. Phys.*, *B 60*, 543.
[39] Macdonald, R., & Eichler, H. E. (1998). In: S. Elston & R. Sambles (Eds.), *The Optics of Thermotropic Liquid Crystals*, Taylor & Francis: London, p. 137.
[40] Eichler, H. J., Macdonald, R., & Trosken, B. (1993). *Mol. Cryst. Liq. Cryst.*, *231*, 1.
[41] Khoo, I.-C.(1995). *Liquid Crystals, Physical Properties and Nonlinear Optical Phenomena*, John Wiley & Sons: New York.
[42] Khoo, I.-C., & Wu, S.-T. (1993). *Optics and Nonlinear Optics of Liquid Crystals*, World Scientifc: Singapore.
[43] Khoo, I. C. (1999). *J. Nonlin. Opt. Mat.*, *8*, 305.
[44] Soileau, M. J., Van Stryland, E. W., Guha, S., Sharp, E. J., Wood, G. L., & Pohlmann, J. L. W. (1987). *Mol. Cryst. Liq. Cryst.*, *143*, 139.
[45] Soileau, M. J., Guha, S., Williams, W. E., Van Stryland, E. W., Vanherzeele, H., Pohlmann, J. L. W., Sharp, E. J., & Wood, G. (1985). *Mol. Cryst. Liq. Cryst.*, *127*, 321.
[46] Hochbaum, A., Fergason, J. L., & Buck, J. D. (1992). *Proc. SPIE*, *1692*, 96.
[47] Hochbaum, A., Hsu, Y. Y., & Fergason, J. L. (1994). *Proc. SPIE*, *2229*, 48.
[48] McEwan, K., & Hollins, R. C. (1994). *Proc. SPIE*, *2229*, 122.
[49] McEwan, K. J., & Hollins, R. C. (1995). *J. Nonlin. Opt. Phys. Mat.*, *4*, 245.
[50] Yuan, H. J., Li, L., & Palffy-Muhoray, P. (1991). *Mol. Cryst. Liq. Cryst.*, *199*, 223.
[51] Palffy-Muhoray, P., Yuan, H. J., Li, L., Lee, M. A., DeSalvo, J. R., Wei, T. H., Sheik-Bahae, M., Hagan, D. J., & Van Stryland, E. W. (1991). *Mol. Cryst. Liq. Cryst.*, *207*, 291.
[52] Kosa, T., Dogariu, A., Palffy-Muhoray, P., & Van Stryland, E. W. (1995). *Opt. Soc. Am. Tech. Dig. Ser.*, *21*, 57.
[53] Zhao, W., & Palffy-Muhoray, P. (1994). *Appl. Phys. Lett.*, *65*, 673.
[54] Palffy-Muhoray, P., Wei, T., & Zhao, W. (1994). *Mol. Cryst. Liq. Cryst.*, *251*, 19.
[55] Li, L., Yuan, H. J., Hu, G., & Palffy-Muhoray, P. (1994). *Liq. Cryst.*, *16*, 703.
[56] Brochard, P., Grolier-Mazza, V., & Cabanel, R. (1997). *J. Opt. Soc. Am.*, *B14*, 405.

[57] Kovsh, D. I., Yang, S., Hagan, D. J., & Van Stryland, E. W. (1999). *Appl. Opt.*, *38*, 5168.
[58] Kovsh, D. I., Hagan, D. J., & Van Stryland, E. W. (1999). *Opt. Express*, *4*, 315.
[59] Lukishova, G. (1999). *Mol. Cryst. Liq. Cryst.*, *331*, 2469.
[60] Sheik-Bahae, M., Said, A. A., Wei, T.-H., Hagan, D. J., & Van Stryland, E. W. (1990). *IEEE J. Quantum Electron.*, *26*, 760.
[61] Palffy-Muhoray, P. (1990). In: B. Bahadur (Ed.), *Liquid Crystals: Applications and Uses*, World Scientific: Singapore, Vol. 1, 493.
[62] Horn, R. G. (1978). *J. Physique*, *39*, 105.
[63] Volterra, V., & Wiener-Avnear, E. (1974). *Opt. Comm.*, *12*, 194.
[64] Wang, P., Zhang, H., & Dai, J. (1988). *Opt. Lett.*, *13*, 479.
[65] Bloisi, F., Vicari, L., Simoni, F., Cipparone, G., & Umeton, C. (1988). *J. Opt. Soc. Am.*, *B5*, 2462.
[66] Lukishova, S. G. (1999). *Proc. SPIE*, *3798*, 128.
[67] Lukishova, S. G. (1999). *Opt. Soc. Am. Tech. Dig. QELS'99*, 126.
[68] Marinelli, M., Mercuri, F., Zammit, U., & Scudieri, F. (1998). *Phys. Rev.*, *E 58*, 5860.
[69] Umeton, C., Cipparrone, G., & Simoni, F. (1986). *Opt. Quantum Electron.*, *18*, 312.
[70] Lukishova, S. G., Lepeshkin, N., Boyd, R. W., & Marshall, K. (2006). *Molec. Cryst. Liq. Cryst.*, *453*, 393.
[71] Lukishova, S. G., Boyd, R. W., Lepeshkin, N., & Marshal, K. L. (2002). *J. Nonl. Opt. Phys. & Mater.*, *11*, 341.
[72] Baals, D. R., & Hess, S. (1985). *Z. Naturforsch.*, *40a*, 3.
[73] Elscher, R., Macdonald, R., Eichler, H. J., Hess, S., & Sonnet, A. M. (1999). *Phys. Rev.*, *E 60*, 1792.
[74] Khoo, I. C., Lindquist, R. G., Michael, R. R., Mansfield, R. J., & LoPresti, P. (1991). *J. Appl. Phys.*, *69*, 3853.
[75] Eichler, H. J., & Macdonald, R. (1991). *Phys. Rev. Lett.*, *67*, 2666.
[76] Akopyan, R. S., Zel'dovich, B. Ya., & Tabiryan, N. V. (1994). *Tech. Phys.*, *38*, 493.
[77] Glorieux, C., Nelson, K. A., Hinze, G., & Fayer, M. D. (2002). *J. Chem. Phys.*, *116*, 3384.
[78] Voloschenko, D., & Lavrentovich, O. D. (1999). *J. Appl. Phys.*, *86*, 4843.
[79] Walls, D. F., & Milburn, G. F. (1995). *Quantum Optics*, Springer Verlag: Berlin, NY.
[80] Knill, E., Laflamme, R., & Milburn, G. J. (2001). *Nature*, *409*, 46.
[81] Lukishova, S. G., Schmid, A. W., Knox, R., Freivald, P., Bissell, L., Boyd, R. W., Stroud, C. R., Jr., & Marshall, K. L. (2007). *J. Mod. Opt.*, *54*(2 & 3), 417.
[82] Lukishova, S. G., Bissell, L. J., Menon, V. M., Valappil, N., Hahn, M. A., Evans, C. M., Zimmerman, B., Krauss, T. D., Stroud, C. R., Jr., & Boyd, R. W. (2009). *J. Mod. Opt.*, *56*(2 & 3), 167.
[83] Lukishova, S. G., Bissell, L. J., Stroud, C. R., Jr., & Boyd, R. W. (2010). *Optics and Spectroscopy*, *108*, 417.
[84] Yamamoto, Y., Santori, Ch., Vuskovic, J., Fattal, D., Waks, E., & Diamanti, E. (2005). *Progr. Informatics*, *2005*(1), 5.
[85] Kopp, V. I., Fan, B., Vithana, H. K. M., & Genack, A. Z. (1998). *Opt. Lett.*, *23*, 1707.
[86] Il'chishin, I., Tikhonov, E., Tishchenko, V., & Shpak, M.(1978). *JETP Lett.*, *32*, 24.
[87] Palffy-Muhoray, P., Cao, W., Moreira, M., Taheri, B., & Munoz, A. (2006). *Phil. Transact. A Math. Phys. Eng. Sci.*, *364*, 2747.
[88] Coles, H., & Morris, S. (2010). *Nature Photonics*, *4*, 678.
[89] Blinov, L. M., & Bartolino, R. (Eds.). (2010). *Liquid Crystal Microlasers*, Transworld Res. Network: Trivandrum.
[90] Chilaya, G., Chanishvili, A., Petriashvili, G., Barberi, R., De Santo, M. P., & Matranga, M. A. (2011). *Scient. Research, Materials Sciences and Applications*, *2*, 116.
[91] Dolgaleva, K., Wei, S. K. H., Lukishova, S. G., Chen, S.-H., Schwertz, K., & Boyd, R.W. (2008). *JOSA B*, *25*, 1496.
[92] Wei, S. K. H., Chen, S. H., Dolgaleva, K., Lukishova, S. G., & Boyd, R. W. (2009). *Appl. Phys. Lett.*, *94*, 041111.

[93] Huang, H., Dorn, A., Bulovic, V., & Bawendi, M. (2007). *Appl. Phys. Lett.*, *90*, 023110.
[94] Lukishova, S. G., Bissell, L. J., Winkler, J., Stroud, C. R., Jr., & Boyd, R. W. (2011). International Conference on Quantum Information, Ottawa, 6–8 June 2011, OSA Technical Digest (CD), paper QWD3.
[95] Bissell, L. J., Lukishova, S. G., & Stroud, C. R., Jr. (2011). Conference on Lasers and Electro Optics (CLEO), Baltimore, May 2011, *OSA Technical Digest* (CD), paper JTuI38.
[96] Lukishova, S. G., Bissell, L. J., Winkler, J., & Stroud, C. R., Jr. (2012). *Opt. Lett.*, *37*, 1259–1261.
[97] Lukishova, S. G., & Schmid, A. W. (2006). *Molec. Cryst. Liq. Cryst.*, *454*, 15–21.
[98] Srinivasarao, M., Collings, D., Philips, A., & Patel, S. (2001). *Science*, *292*, 79.
[99] Golovataya, N. M., Kurik, M. V., & Lavrentovich, O. D. (1990). *Liquid Cryst.*, *7*, 287.
[100] Widawski, G., Rawiso, M., & Francois, B. (1994). *Nature*, *369*, 387.